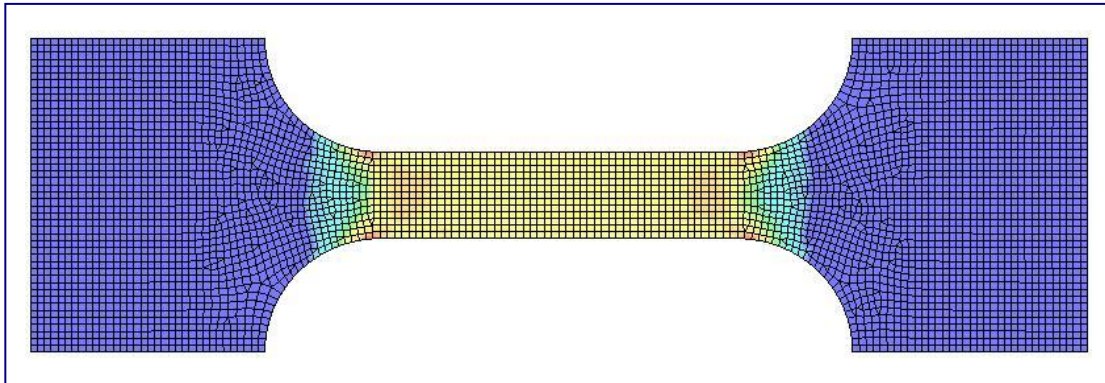


# CHALMERS



## Finite Element Simulation: Tensile test of rib cortical bone

AINHITZE MENDIZABAL DONES

Department of Applied Mechanics  
*Division of Vehicle Safety*  
CHALMERS UNIVERSITY OF TECHNOLOGY  
Göteborg, Sweden 2010  
Master's Thesis 2010:04



MASTER'S THESIS 2010:04

Finite Element Simulation:  
Tensile test of rib cortical bone

AINHITZE MENDIZABAL DONES

Department of Applied Mechanics  
*Division of Vehicle Safety*  
CHALMERS UNIVERSITY OF TECHNOLOGY  
Göteborg, Sweden 2010

Finite Element Simulation: Tensile test of rib cortical bone

AINHITZE MENDIZABAL DONES

© AINHITZE MENDIZABAL DONES, 2010

Master's Thesis 2010:04

ISSN 1652-8557

Department of Applied Mechanics

Division of Vehicle Safety

Chalmers University of Technology

SE-412 96 Göteborg

Sweden

Telephone: + 46 (0)31-772 1000

Cover:

The effective plastic strain levels in a shell specimen simulated in Ls-Dyna

Department of Applied Mechanics

Göteborg, Sweden 2010

Finite Element Simulation: Tensile test of rib cortical bone  
ANHITZE MENDIZABAL DONES  
Department of Applied Mechanics  
Division of Vehicle Safety  
Chalmers University of Technology

## ABSTRACT

Thoracic trauma is the principal causative factor in 30% of road traffic deaths [1]. And when 6 or more ribs are fractured, mortality rate and associated injuries to the head and thorax are increased significantly [2].

This thesis work was carried out to improve the understanding of the mechanical properties of the human rib. These properties are necessary in order to develop realistic finite element models of human chest which are used in the field of vehicle safety.

The purpose of this study was to collect values for the rib mechanical properties obtained experimentally. And to compare the values of material properties of human rib cortical bone used in the FE simulation of THUMS with the material properties of human rib cortical bone of PMHS analyzed by Kemper et al. with a tensile test [3].

It has been simulated a tensile test of a specimen of cortical bone of the rib with a FEM in Ls Dyna. The cortical bone has considered a piecewise linear plasticity material and it has been simulated with shell elements. The specimen was loaded at a rate of 5 mm/s (0.5 strains/s). The results of the traction test have been compared with those of Kemper et al. realized on six PMHS. It has been observed that the FE model results are closer to the experimental results if strain rate parameters are not used.

Key words: Finite Element Method, cortical bone, stress, strain.



# Contents

ABSTRACT	I
CONTENTS	III
PREFACE	V
1 INTRODUCTION	1
2 BACKGROUND	3
2.1 Injuries in thorax	3
2.2 Anatomy of chest	5
2.2.1 Rib cage	5
2.2.2 The rib: cortical and trabecular bone	6
2.2.3 Mechanical properties of ribs	7
2.2.4 Assumptions of mechanical properties of ribs in FEM	9
3 MATERIALS AND METHODS	21
3.1 Cortical bone tests	21
3.2 Tensile tests on PMHS (Kemper et al. 2005)	21
3.2.1 Specimen preparation	22
3.2.2 Testing configuration	24
3.2.3 Results	24
3.3 FEM simulation in Ls-Dyna	26
3.3.1 Specimen preparation	26
3.3.2 Testing configuration	27
3.3.3 Material properties of human rib cortical bone in FEMs	28
3.3.4 Material type	29
3.3.5 Mesh: Element size	30
3.3.6 Results	35
3.3.7 Influence of strain rate	39
3.3.8 Effective plastic strain	43
3.3.9 Comparison with results of Kemper 2005	44
4 DISCUSSION	47
5 FUTURE WORK	48
6 CONCLUSION	49
7 REFERENCES	50
8 APPENDIX	53

8.1	Stress - strain curves of cadaver 2 (male of 45 years old) and cadaver 6 (male of 18 years old) obtained by Kemper	53
8.2	Simulation of tensile test. Shell element of 0.2 mm and strain rate of 0.5 strains/s.	57
8.3	THUMS model	61

## **Preface**

This Master's Thesis was carried out at SAFER Vehicle and Traffic Safety Centre at Chalmers, in Göteborg, Sweden. The work was carried out from September 2009 to February 2010.

I would like to thank Johan Davidsson, my examiner, Karin Brolin, for her help in tough times. And especially, I would like to thank Manuel Mendoza-Vazquez, my supervisor, for his continued support in this work.

Göteborg, February 2010

Ainhitze Mendizabal Dones



## **Abbreviations**

FE: Finite Element

FEM: Finite Element Method

THUMS: Total Human Model for Safety

PMHS: Post Mortem Human Subject

CIREN: Crash Injury Research and Engineering Network

ATD: Anthropomorphic Test Device

AIS: Abbreviated Injury Scale

AAAM: Association for the Advancement of Automotive Medicine

NASS: National Automotive Sampling System



# 1 Introduction

The thorax contains the primary elements of the respiratory and circulatory systems. A variety of critical physiological processes occur in there. Thoracic trauma is the principal causative factor in 30% of road traffic deaths [1]. In automobile crashes, thoracic injuries rank second only to head injuries in three categories: In the area most often injured, in the overall number of fatalities and serious injuries and in the overall societal harm [4].

Rib fractures and flail chests are the most frequent types of thoracic injuries for both drivers and passengers, followed by pulmonary, liver and arterial injuries [3]. Data from the Crash Injury Research and Engineering Network (CIREN) showed that rib fractures were the most serious injury sustained by 40% of the patients over 60 who died of chest injuries from automobile collisions [5]. Increasing the number of rib fractures correlated directly with increasing mortality. Patients sustaining fractures of 6 or more ribs are at significant risk for death from causes unrelated to the rib fractures. When six or more ribs are fractured, mortality rate and associated injuries to the head and thorax are increased significantly [6]. Studies using restrained cadavers in impact sled tests have frequently found rib fractures to be the most common skeletal injury [7].

It is important to develop a method to reduce these injuries. This requires investigate injury mechanisms, to predict human body response to impact. One of the most important human body responses to evaluate during the impact is the occurrence of rib fractures under various impact situations. The capability to predict rib fractures occurring under different loading conditions would give a great help for further development of car safety.

Anthropomorphic test devices (ATDs), finite element (FE) computer models, and other models are commonly used to evaluate the safety of vehicle and the human response to automobile crash loading. Current crash dummies were developed in order to measure the forces acting on a human body. They were validated for a specific type of impact and as a consequence their application is limited. Moreover, dummies are limited in their biofidelity. Some authors affirm that anthropometric test devices (ATDs) cannot explain the complex mechanics because their limited instrumentation and macro-level injury criteria [8].

Nowadays, Human Body Finite Element Models (FEMs) play an increasingly important role in vehicle safety system design for injury mitigation. FEM, as a powerful numerical tool is of a great value in this regard. These computational models can be used as a substitute for experimental measurements. Numerical human modeling allows for the calculation of physical variables mechanically related to injury, and it analyze strains and stresses locally, which helps in predicting the injury response in car occupant crashes. These models can be used for the analysis of injury mechanisms, to study the tolerance of the human body to impact, and car crash reconstruction. Finite element models of human thorax are becoming an integral tool in the reduction of these injuries, thereby improving crashworthiness.

However, the validation of these models remains very coarse. At this time, they do not adequately model detailed mechanisms of injuries such as rib fractures. One of the main barriers is the large degree of complexity of bone. Its mechanical behavior depends on the bone type, age, gender, its anisotropic mechanical behavior and strain rate dependency. So, designing a model to be biofidelic for different types of loading and capable to accurately predict injury, requires focusing more locally on material properties. The correct biomechanically-based material properties must be applied.

The aim of this study is to redefine the material parameters of the rib cortical bone of the THUMS (Total HUMAN Model for Safety) Finite Element Model. THUMS is a computational model to simulate motions and stress or strain distributions of the human whole body for impacts. THUMS represents a mid size adult male (it has a height of 1.75m, a weight of 77kg, and an age of 30's – 40'). The THUMS model was developed by Toyota Motor Corporation and Toyota Central R&D Labs. [9].

## 2 Background

### 2.1 Injuries in thorax

The thorax contains the primary elements of the respiratory and circulatory systems, and the rib cage protects several abdominal organs, including the liver, spleen, kidney, and stomach [10]. Crash injuries of the chest are either fatal within a brief time period or not; there are few long term consequences: Almost everything that resides in the chest, such as the heart and lungs, and nearly everything that transits the chest on the way to somewhere else, such as lymph and nerve trunks, the esophagus, vena cava, and the aorta and its branches, these items and organs may be considered vital, which is to say damaging them will often be fatal [11].

The standard method for assessing the severity of the wounds of a body segment or organ is the AIS scale. The AIS score varies between 0 and 6; 0 (no injury) to 6 (maximum, virtually unsurvivable), as there is in the table 1. The higher the AIS level, the higher the chance of life threatening injuries and mortality. The scale does not reflect the evolution of injury over time, nor the medical and societal costs of these.

AIS	Severity code	Skeletal Injury
0	No injury	-
1	Minor	1 rib fracture
2	Moderate	2-3 rib fractures; sternum fracture
3	Serious	4 or more rib fractures on one side; 2-3 rib fractures with hemothorax or pneumothorax
4	Severe	Flail chest; 4 or more rib fractures on each of two sides; 4 or more rib fractures with hemo or pneumothorax
5	Critical	Bilateral flail chest
6	Maximum injury (virtually unsurvivable)	-

Table 1: AIS rating for skeletal thoracic injuries [AAAM 2005]

It was examined incidence of injuries due to frontal impacts in the National Automotive Sampling System (NASS) from 1988 to 1994, and it was found that chest injuries constituted 37.6 % of all AIS 3+ injuries, 46.3 % of all AIS 4+ injuries, and 43.3 % of all AIS 5+ injuries [7]. Thorax injuries have been shown to account for approximately 13% of all AIS 1-2 injuries and 29% of all AIS 3-6 injuries [4]. It was showed that 47 % of drivers over 64 years of age, 33 % of drivers age 34 through 64, and 24 % of drivers age 16 through 33 who died in a frontal crash sustained a fatal chest injury [7].

The pleural cavity is an enclosed space. To keep the lung in their inflated state, a continuous underpressure is maintained in the pleural cavity [12]. If not, can occur several injuries like:

#### Pneumothorax:

If this underpressure cannot be maintained (for example due to a perforation of the chest), the lungs will deflate and the pleural cavity will be filled with air.

#### Hemothorax:

The pleural cavity is filled with blood.

#### Hemo-pneumothorax:

The pleural cavity contains both blood and air.

#### Injuries to internal structures:

Due to the restricted space available in the mediastinum, a compression of the anterior rib cage may easily cause injuries to internal structures. If the thorax is suddenly decelerated due to a blunt impact, three different injury mechanisms can be distinguished: compression, viscous loading and inertia loading of the internal organs.

Furthermore, any combination of those three basic phenomena can occur.

#### Rib fractures:

Closed fracture: The skin and the soft tissue overlaying the fracture remain intact.

Open fracture: Sharp edges of broken ribs perforate the chest wall. These fractures can lead to a pneumothorax, lung collapse and infections.

Broken ribs may also perforate the visceral or parietal pleura, causing respiratory problems.

#### Lung injuries:

Due to thorax compression (both with and without rib fracture) a lung contusion can occur. This often happens in combination with a flail chest.

Unlike rib fractures, lung contusion is rate dependent. At high velocities, a compression or pressure wave is transmitted through the thorax wall to the lung tissue, causing damage to the capillary bed of the alveoli.

#### Injuries to other thoracic organs:

From thoracic impact, the heart can be subjected to several injuries including contusion and laceration. Contusion occurs due to compression and depends on the associated velocity. Laceration may be due to high magnitude of compression over the sternum. At high rates of loading, the heart may undergo arrhythmia, fibrillation or arrest.

## 2.2 Anatomy of chest

### 2.2.1 Rib cage

The ribcage consists of the spine, sternum and 12 pairs of ribs with their cartilage, as in Figure 1. Each rib articulates with respect to the vertebrae to facilitate respiration. The anterior surface is formed by the sternum and costal cartilage. The costal cartilages form a bridge between the central sternum and the ribs.

The first seven sets of ribs are connected directly to the sternum by the costal cartilage, the following three pairs join together by costal cartilage then attach to the sternum, and the last two are floating ribs, they are attached to the vertebrae only.

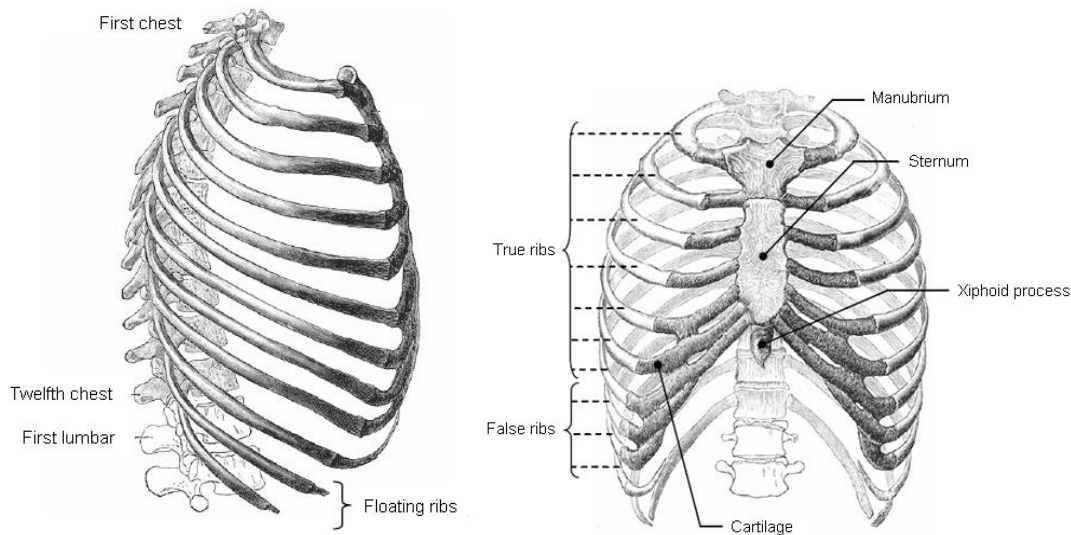


*Figure 1: Rib cage [13]*

Figure 2 shows the different parts of a rib.

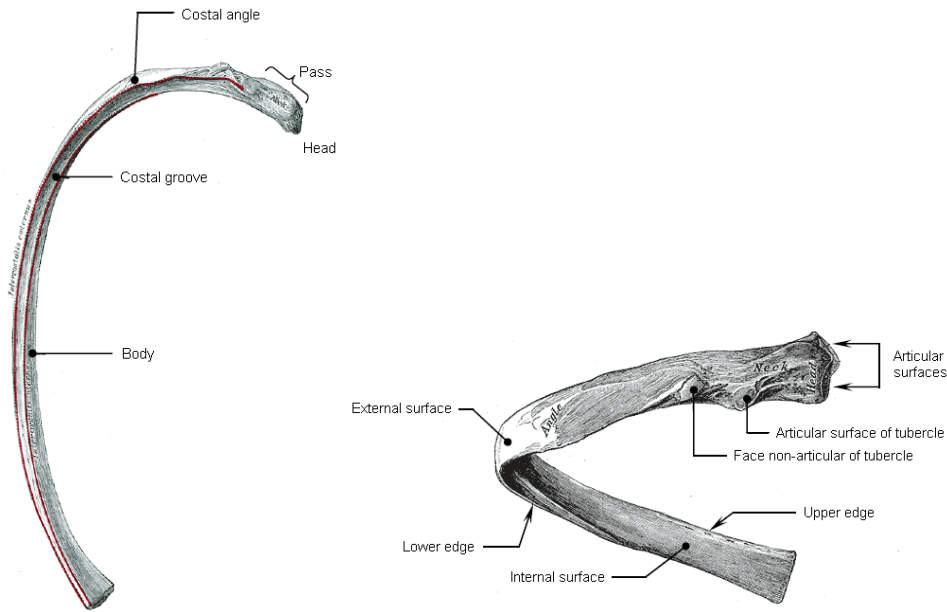


Figure 2: Rib [13]

### 2.2.2 The rib: cortical and trabecular bone

The ribs themselves are composed of cancellous (spongy or trabecular) bone surrounded by a cortical shell, as in the Figure 3.

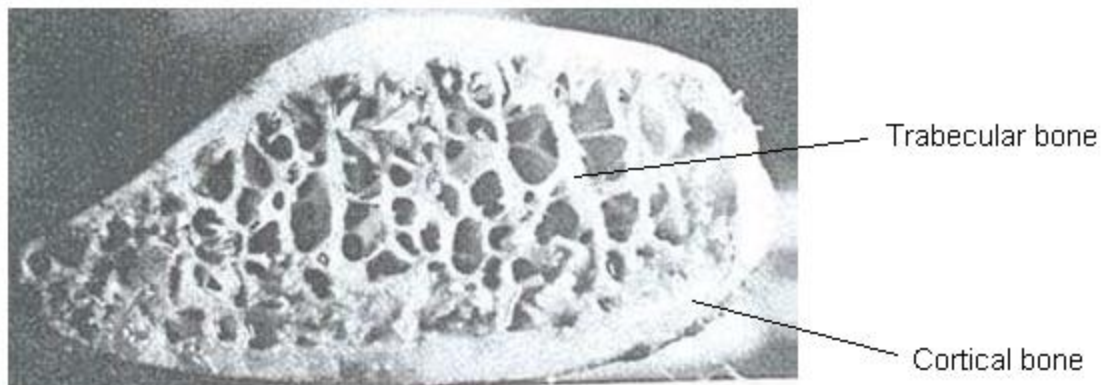


Figure 3: Photography under UV [13]

The cortical bone is a compact bone. It is solid, strong and resistant to bending and compression [14]. It is the primary load carrying material in long bones [2]. It is a dense material comprising the walls of shaft of long bones and external surfaces of bones. The thickness of cortical bone varies between and within bones [14].

The cancellous bone of the interior region of ribs, is formed from the thin bony spicules, also called trabeculae. Between them there are irregular interconnecting spaces,

reducing the weight of the bone. Cancellous bone has a higher surface but is less dense and less stiff than compact bone and it is more resistant to compressive and tension loads in comparison with shearing [14].

### 2.2.3 Mechanical properties of ribs

In the literature reviewed for this project it was found that the Young's modulus of rib bone varies from 1.27 to 50.6 GPa and that the Young's modulus of rib cortical bone varies from 7.51 to 20 GPa. Some authors affirmed that the Young's modulus of cortical bone varies from 15 to 35 GPa and others ones that it is about 20-22 GPa along the axis of long bone and about 12-14 GPa transversely [13]. The Young's modulus of cancellous bone varies from 1.4 to 9800 MPa [13] or from 1 to over 20 GPa [15]. This wide range in the values of the elastic modulus is due to a lot of factors that affect the values of mechanical properties measured experimentally. The values of mechanical properties depend on the type of test (tensile, compressive, bending, shear, etc), on the characteristics of the tested subject (age, gender, weight, bone mineral density, etc) rib level and location of the specimen, on the type of subject (cadaver or living human), the load distribution, and so on.

The cortical bone structure is very compact, heterogeneous, viscoelastic and anisotropic [13]: Bone has heterogeneous structure; it means that the properties vary with the point. Bones have viscoelastic properties; it means that the mechanical behavior depends on the speed at which the load is applied. The higher the strain rate is the higher the stress at a given strain [14]. Bone is also an anisotropic material; it means that it has different mechanical properties when loading is applied along different axes. It is caused by the structure of bone, which is dissimilar in the transverse and longitudinal directions [14]. The Young's modulus of cortical bone in the longitudinal or axial direction ( $E_L$ ) was about 40% greater than the Young's modulus in the transverse direction ( $E_T$ ) [15]. It was presented one of the human cortical bone material property studies using coupons taken from human femur and tibia bones. This study conducted tension and compression tests in both the axial and lateral directions. The results showed that the ultimate stress and strain were significantly lower in the lateral direction than in the axial direction, thereby defining cortical bone as a non-isotropic material. However, only quasi-static loading rates were tested. These tests were conducted at quasi-static rates and did not examine viscoelastic effects [3]. Some authors assumed that the material properties of the rib have elastic-plastic characteristics. However, others studies found no plastic behavior in the cortical bone [16]. The compact bone exhibits inelastic responses that differ in tension and compression. In compression, cortical bone yields at higher stress than in tension [17] [18], and the ultimate stress and strain at break are higher in compression [13] as in Figure 4. So, this observation suggests that the rupture of the compact bone is determined by its ability to withstand tensile loading.

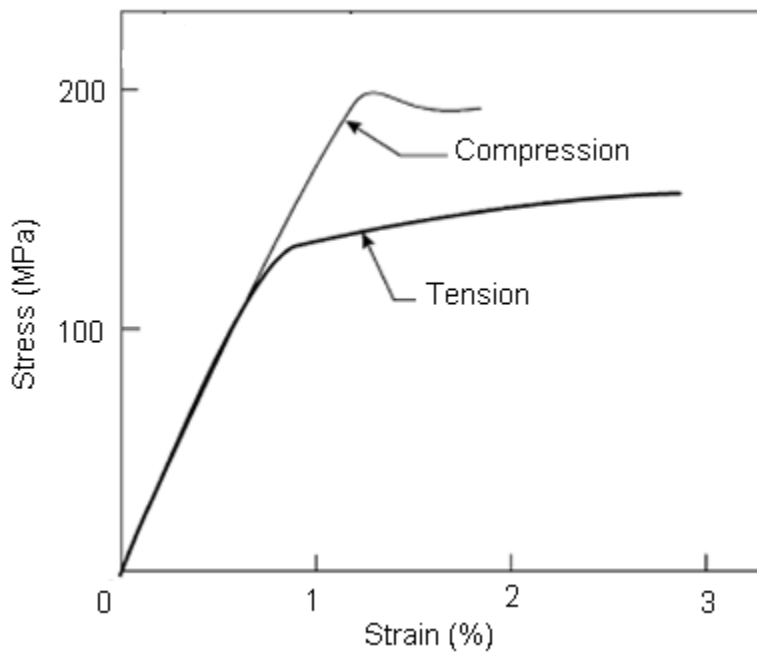


Figure 4: Schematic of the tensile and compressive stress/strain curves for cortical bone along the axis of a long bone.

It was founded that the cortical bone has a tensile modulus lower in compression than tension [13] as in the Figure 5.

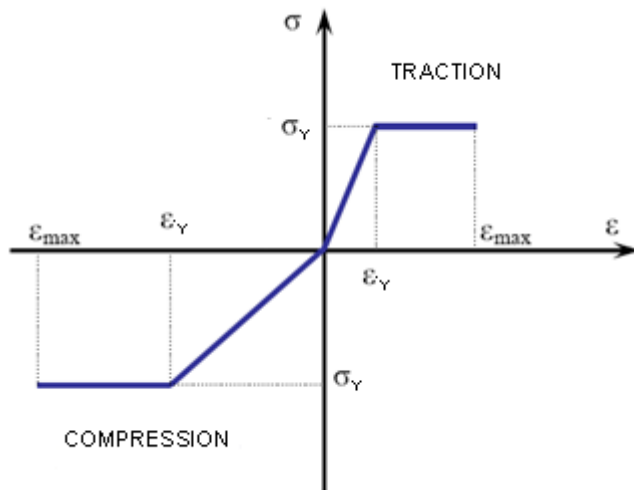


Figure 5: Theoretical law of behavior of compact bone, of tensile and compressive.

In tests on human femoral diaphyses, Kaneko et al. found that yield stress, failure stress, Young's modulus, and yield deformation were lower with traction than with compression. On the other hand, deformation at failure was greater with traction.

Thus, plastic cortical bone deformation is more marked with traction than with compression [1].

Trabecular bone is quite heterogeneous, viscoelastic and anisotropic. The yield point of trabecular bone differs during traction and during compression, and traction stress is about 50% less than compression stress [1]. When compressed, trabecular bone exhibits extensive inelastic deformation (Figure 6), often attaining strains exceeding 60% before failure [17].

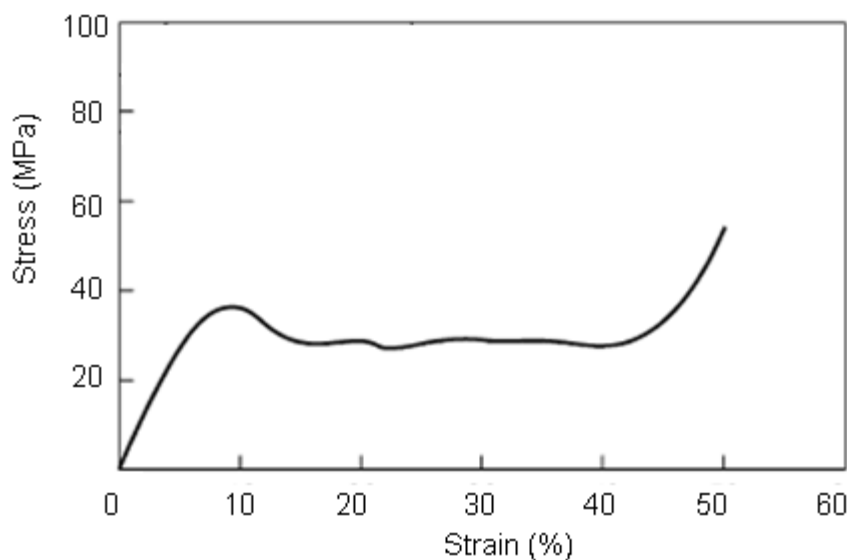


Figure 6: Schematic of a compressive stress/strain curve for trabecular bone

In regard to the entire rib bone, it was concluded that the bone did not exhibit a different behavior in tension than compression but, that the fracture occurs first in tension [4].

#### 2.2.4 Assumptions of mechanical properties of ribs in FEM

In the THUMS model rib bone is considered homogeneous, isotropic, linear elastic with plastic zone and viscoplastic.

### 2.3 Summary of articles of tests of bones

Ref	Author	Test type	Subject	Specimen type	Specimen length	Load direction	Strain rate
[3]	Dempster and Lippicoat (1952)	Traction and compression	Human	Femur and tibia bones		Axial and lateral	Quasi-static
[3]	Evans and Bang (1956)	Traction	Human	Femur, tibia and fibula cortical bone		Axial	Quasi-static
[3]	McElhaney and Byars (1965)	Compression	Human	Femur bone		Axial	Various loading rates
[13]	Wood (1971)	Traction		Cranial bone		Axial	0.005 - 150 s <sup>-1</sup>
[3] [13]	Stein and Granik (1973)	3 point bending	15 cadavers	Whole rib sections (6 <sup>th</sup> and 7 <sup>th</sup> ribs)	152 mm		
[13]	Schultz et al (1974)	Solicitation multidirectional	5 males (29 – 43 years old)	Whole rib + Cartilage (2 <sup>nd</sup> , 4 <sup>th</sup> , 6 <sup>th</sup> , 8 <sup>th</sup> , 9 <sup>th</sup> and 10 <sup>th</sup> ribs)			Static
[3]	Reilly and Burstein (1975)	Traction	Human	Femur bone		0°, 30°, 60° and 90° from the transverse plane	Quasi-static

[13]	Got et al (1975)	3 point bending	34 cadavers (24 – 94 years old)	Rib specimen (5 <sup>th</sup> and 6 <sup>th</sup> ribs)	80 mm		Static: 1 mm/min Dynamic: 3 m/s
[13]	Got et al (1975)	Shear	34 cadavers (24 – 94 years old)	Rib specimen (5 <sup>th</sup> and 6 <sup>th</sup> ribs)	40 mm		1 mm/min
[3]	Saha and Hayes (1976)	Traction				Axial	Dynamic
[13]	Stein and Granik (1976)	3 point bending	79 cadavers (27 – 83 years old)	Whole rib sections (6 <sup>th</sup> and 7 <sup>th</sup> rib)	152 mm		0.508 mm/min, 2.54 mm/min, 12.7 mm/min
[13]	Carter and Hayes (1976, 1977)	Compression	Human tibia and bovine femur	cylindrical samples		Axial	0.0005 - 250 s <sup>-1</sup>
[13]	Kallieris et al. (1979)	3 point bending	66 cadavers (44 males and 20 females) (12 – 74 years old)	Rib specimen (6 <sup>th</sup> and 7 <sup>th</sup> rib)	200 mm		2.5 mm/min
[13]	Sacreste et al. (1981)	3 point bending		Whole rib sections (5 <sup>th</sup> and 6 <sup>th</sup> rib)	80 mm		1 mm/min
[13]	Cesari and Bouquet (1981)	3 point bending	6 cadavers (71 years old)	Rib specimen (5 <sup>th</sup> and 6 <sup>th</sup> rib)	70 - 120 mm		1 mm/min

[13]	Verriest and Chapon (1985)	Ring rib compression	1 male (53 years old)	2 ribs + Cartilage + Sternum + Vertebrae			
[13]	Rumelhart et al (1987)	Compression	4 cadavers	Rib specimen (3 <sup>rd</sup> , 5 <sup>th</sup> , 6 <sup>th</sup> , 7 <sup>th</sup> and 8 <sup>th</sup> ribs)	25 mm	Axial	$0.625 \cdot 10^{-3} \text{ s}^{-1}$
[13]	Rumelhart et al (1988)	Ring rib compression	2 males (50 – 53 years old)	2 ribs + Cartilage + Sternum + Vertebrae		Axial	$0.625 \cdot 10^{-3} \text{ s}^{-1}$
[13]	Schaffer and Burr (1988)	Traction (in the elastic zone without break)	Beef femoral diaphysis and tibia	Cylindrical samples of compact bone		Axial	$0.01 - 0.03 \text{ s}^{-1}$
[13]	Currey (1988)	Traction	Different animal species	Cortical bone		Axial	$0.2 \text{ s}^{-1}$
[13]	Currey (1988)	3 point bending	Different animal species	Cortical bone			$0.001 \text{ s}^{-1}$
[13]	McCalden et al. (1993)	Traction	Humans (20 – 102 years old)	Cortical bone of femur		Axial	$0.03 \text{ s}^{-1}$
[13]	Keller (1994)	Compression	Humans (46 – 84 years old)	Vertebral and femoral bone (Cubic specimens)		Axial	$\sim 0.01 \text{ s}^{-1}$
[19]	Yoganandan and Pintar (1998)	3 point bending	30 cadavers (29 – 81 years old)	Whole rib sections (7 <sup>th</sup> and 8 <sup>th</sup> rib)	150 mm		2.5 mm/min

[13]	Kallieris (2000)	3 point bending	11 cadavers (20 – 70 years old)	Rib specimen (6 <sup>th</sup> and 7 <sup>th</sup> rib)			Static: 2.5 mm/min Dynamic: 2 m/s and 4 m/s
[13]	Kallieris (2000)	Compression		Rib specimen (5 <sup>th</sup> and 6 <sup>th</sup> rib)	30 mm	Axial	4 m/s
[18]	Vashishth et al. (2000)	Axial (Traction and compression) and Torsion	38 bovines (18 months - 2 years old).	Tibiae (Cylindrical specimens)	62 mm (22 mm usefult)		0.03 s <sup>-1</sup>
[20]	Akhter et al. (2000)	3 point bending	Female rats	Tibiae and femora	Femora:~14mm Tibiae:~18mm		3 mm/min
[21]	Lind et al. (2001)	Torsion	68 female rats	Humeri			4 °/s
[22]	Kimpara et al (2003)	3 point bending	96 cadavers (70 males and 26 females)	Rib specimen (6 <sup>th</sup> and 7 <sup>th</sup> rib)			1 mm/min
[23]	Stitzel et al. (2003)	3 point bending	4 cadavers (2 males and 2 females) (61 – 71 years old)	Rib cortical bone specimen (from 2nd to 12th rib)	Small rectangular coupons: 29mm		356 mm/s

[24]	Kaneko et al. (2003)	Traction - Compression	9 cadavers	Femoral diaphyses	15 mm (6 mm usefals)	Axial	0.1% strains/s
[25]	Goss et al. (2003)	3 point bending	Female rats	Lumbar vertebrae and femora			2 mm/min
[26]	Neil Dong (2003)	Traction and Torsion	1 male (64 years old) and 2 females (44 and 60 years old)	Femoral cortical bone	20 mm (10 mm usefals)	Longitudinal and transverse	Traction: 0.1% strains/s Torsion: 1°/s
[27]	M. Pithioux et al (2004)	Traction	Bovines (5-7 years old)	Femoral cortical bone	100 mm (60 mm usefals)	Axial	Quasi-static: 0.5, 5, 10 and 500 mm/min Dynamic: 1m/s
[3]	Cornier et al. (2005)	3 point bending	4 cadavers (2 males and 2 females) (61 - 71 years old)	Whole rib sections (from 2nd to 12th rib)			
[3]	Kemper (2005)	Traction	6 cadavers: 3 males and 3 females. (18 - 67 years old)	Rib specimen (from 1st to 12th rib)	30 mm (10 mm usefals)	Axial	Dynamic: 0.5 strains/s 5 mm/s
[13]	Charpail (2005)	3 point bending	6 cadavers (54-73 years old)	Whole rib (from 6 <sup>th</sup> to 9 <sup>th</sup> ribs)			0.10 m/s and 0.25 m/s

[13]	Charpail (2005)	Compression	6 cadavers (54-73 years old)	Cortical bone (from 6 <sup>th</sup> to 9 <sup>th</sup> ribs)	25 mm	Axial	0.2 and 0.5 s <sup>-1</sup>
[13]	Charpail (2005)	Compression anteroposterior	5 cadavers: 3 males and 2 females (58 – 70 years old)	Ribs (from 4 <sup>th</sup> to 9 <sup>th</sup> rib)			~ 0.22 – 0.6 s <sup>-1</sup>
[17]	C. Mercer et al (2006)	4 point bending	Bovines	Femur	40 mm		0.5 mm/min
[28]	M. Bessho et al (2007)	Compression	11 cadavers: 5 males (30-90 years old) and 6 females (52-85 years old)	Femur		Femur slated at 20° in the coronal plane	Quasi-static: 0.5 mm/min
[7]	Kemper (2007)	3 point bending	6 male cadavers (42 – 81 years old)	Whole rib sections (from 4th to 7th rib)	10.16 cm		0.7 strains/s
[7]	Kemper (2007)	Traction	6 male cadavers (42 – 81 years old)	Isolated cortical bone of rib (from 4th to 7th rib)	30 mm (10 mm usefulls)	Axial	0.5 strains/s
[29]	Arregui-Dalmases et al (2008)	Compression	14 cadavers (14 – 56 years old)	Clavicles		Axial	Quasistatic: 0.63 mm/s

[29]	Hansen et al (2008)	Traction	1 cadaver: Male (51 year old)	Femur	12 mm	Axial	1 mm/s, 10 mm/s, 50 mm/s, 100 mm/s and 200 mm/s
[30]	Hansen et al (2008)	Compression	1 cadaver: Male (51 year old)	Femur	7 mm	Axial	1 mm/s, 10 mm/s, 50 mm/s, 100 mm/s and 200 mm/s

*Table 2: Literature review on tests of bones.*

## 2.4 Summary of mechanical properties of the rib bone

Ref	Subject	Test	Specimen	E [GPa]	$\sigma_{ult}$ [MPa]	$\epsilon_{ult}$	Def [mm]	K [N/mm]	$F_{max}$ [N]
Granik and Stein (1973)	15 cadavers	3 point bending	Rib specimen	11.5	106	0.41 cm			
Got et al (1975)	34 cadavers (24-94 years old)	3 point bending	Rib specimen	Stat.: 7.807±4.05	Stat.: 109±61		Stat.: 6.23±2.84 ; Dyn.: 4.62±1.13	Stat.: 154.8±86	Stat.: 192.2±95.2; Dyn.: 117.8±58.5
Sacreste et al (1981)		3 point bending	Rib specimen	6.14±4.26	86±55				
Cesari and Bouquet (1981)	6	3 point bending	Rib specimen				3.30±0.82		210±134
Yoganand an and Pintar (1998)	30 cadavers (29-81 years old)	3 point bending	Rib specimen	2.32	188.6				

Kallieris (2000)	11 cadavers (20-70 years old)	3 point bending	Rib specimen	10.113±4.529; 12.872±3.421; 9.561±2.431	110±59; 287±72; 206±77	Stat.: 3.7±1.2	2 m/s: 569±92; 4 m/s: 460±110
Kimpara et coll. (2003)	70 males 26 females	3 point bending	Rib specimen	F: 7.57±5.44; M: 7.21±5.94		F: 44.3±27.3 ; M: 216±107	F: 149±79; M: 216±107
Cornier et al (2005)	4 cadavers	3 point bending	Rib specimen	Ant.: 7.51; Lat.: 11.9; Post.: 10.7 Average: 17.7	Ant.: 116.7; Lat.: 153.5; Post.: 127.7 Average: 135.4	Average : 1.38 %	
Charpail (2005)	6 cadavers (54-73 years old)	3 point bending	Whole rib	Static: 9; Dynamic: 11; Ant: 7.51; Med: 11.9; Post: 10.7; Average: 12.72	Static: 110; Dynamic: 250; Ant: 117; Med: 153; Post: 128 Average: 179	4.9	59 216

Charpail (2005)	5 cadavers (58-70 years old)	Lateral compression	Whole rib	~13	150				
Rumelhart et comm. (1987)		Compression	Rib specimen	9.32-50.6	27-197				
Kallieris (2000)		Compression	Rib specimen	2.7	105.3				
Ashman et al (1984)		Continuous wave acoustic technique	Cortical specimen	Longitudinal: 20 Transverse: 13.4					
Stützel et al (2003)	4 cadavers (61-71 years old)	3 point bending	Small cortical bone coupons	Ant.: 7.51; Lat.: 11.9; Post.: 10.7	Ant.: 116.7; Lat.: 153.5; Post.: 127.7				

Kemper et al. (2005)	6 cadavers : 3 males and 3 females (18 – 67 years old)	Traction	Cortical specimen	13.96±3.76	124.2				
----------------------	--	----------	-------------------	------------	-------	--	--	--	--

Table 3: Literature review on mechanical properties of rib bone.

The Young's modulus of the rib specimen varies from 1.27 GPa to 17.7 GPa in the three-point bending tests, and from 2.7 GPa to 50.6 GPa for the axial compression tests.

The Young's modulus of the rib cortical bone varies from 7.51 GPa to 11.9 GPa in three-point bending tests and from 10.2 GPa to 17.72 GPa in a tensile test.

## **3 Materials and methods**

### **3.1 Cortical bone tests**

From the literature survey done during this project, two types of tests to evaluate the material properties of human rib cortical bone were identified. These types of tests were three-point bending and tensile tests. Although three-point bending provides the overall structural response of human rib sections, there are inherent limitations that introduce uncertainty in the calculated material properties [7]. The most important is the necessity to calculate stress, strain and modulus with linear elastic beam equations that do not take plasticity into account. As a result, the calculated stress at failure will be too high [3]. It is because of cross sectional area variations affecting load distribution during bending, that yielding of the tensile and compressive surfaces in a bending test creates a difference between the actual and predicted stress. It was found that linear elastic beam equations can overestimate the ultimate stress by 50 to 100 percent, and it was suggested that ultimate stress determined from 3 point bending tests could be corrected by dividing by a factor of 1.56 for rectangular cross sections and 2.1 for circular cross sections [3] [23]. So, tension testing avoids the need to calculate material properties based on equations that assume linear elastic behavior and the subsequent correction factors needed to account for plasticity. During the three-point bending test, the strain is measured directly, however, the measured ultimate strain may be lower than the true ultimate strain, depending on the location of the fracture relative to the strain gage [3] and the elastic modulus may be overestimated [7]. Three-point bending tests will always be limited by the need to calculate the stress and strain, which requires assumptions and correction factors, rather than measuring them directly.

Therefore, the ideal method for determining the material properties of cortical bone is tension or compression testing performed on isolated cortical bone coupons [7]. In compression, cortical bone yields at higher stress than in tension, so, the fracture occurs first in tension. This is why it was decided to simulate a tensile test in order to compare the rib cortical bone material properties of THUMS with tests performed on human ribs.

### **3.2 Tensile tests on PMHS (Kemper et al. 2005)**

To get more realistic results as possible, it has been sought to compare the simulation test with a real test with cadavers. As previously described, the tensile test is a more reliable test to evaluate the material properties of rib cortical bone. Therefore, the results from tensile tests were used as a basis for comparison. The tensile tests used in this project correspond to the tests conducted by Kemper et al. In the following lines, these tests are described.

### 3.2.1 Specimen preparation

In this study material properties of human rib cortical bone were developed using dynamic tension coupon testing. This study presents 117 human rib cortical bone coupon tests from six cadavers, three male and three female, ranging in age from 18 to 67 years old.

Table 4 shows the osteogram data of these cadavers. The bone mineral density (BMD) of each cadaver was determined by the Osteogram technique. The left hand of the cadavers was x-rayed. This type of BMD measurement, however, only provides an indication of overall bone strength and does not account for local changes in bone density or composition.

Cadaver	Gender	Age	Global BMD
1	Female	64	89.2
2	Male	45	81.4
3	Male	67	105.4
4	Female	61	122.3
5	Female	46	93.7
6	Male	18	138.3

Table 2: Osteogram data for cadavers used in rib cortical bone testing.

The rib cage was removed from the body. The rib sections were taken from the anterior, lateral, and posterior regions on ribs 1 through 12 of each cadaver's rib cage, as in Figure 7.

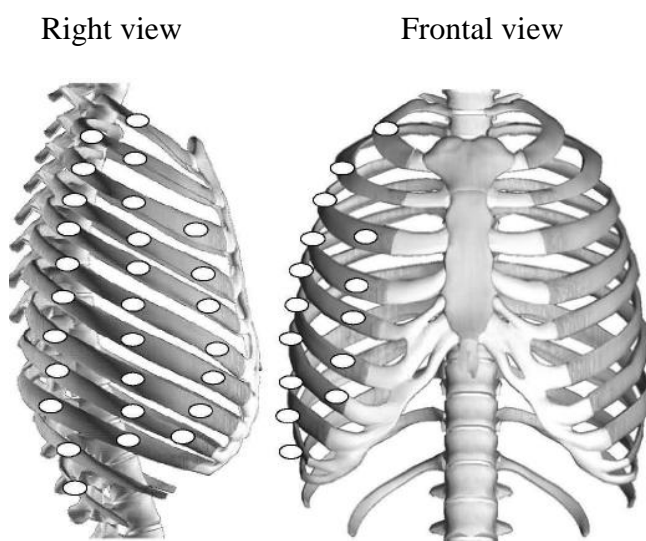


Figure 7: The locations of the rib specimens (anterior and lateral shown twice).

Rectangular coupons from the rib section were cut with micrometer precision (Figure 8).

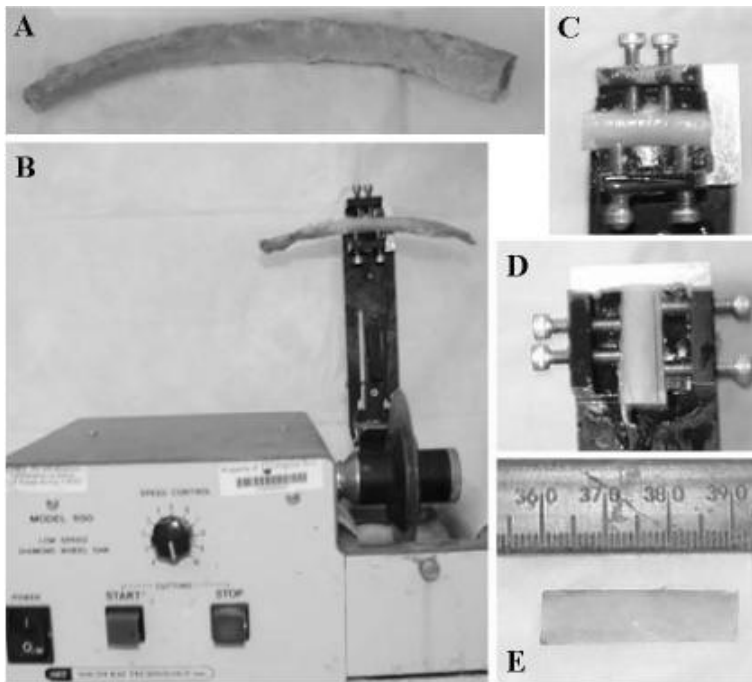


Figure 8: A) Anterior, lateral and posterior sections were cut from each rib of the cage. B) Rib sections were placed in a bone chuck and mounted to the low speed diamond saw. C) Specimen were cut to the final specimen length. D) Two parallel cuts were made on the exterior side along the axis of the rib to obtain the final specimen width. E) Rib coupon cut to final dimensions and ready for milling.

The proper specimen hydration was maintained at all times during preparation and testing. The tissue and periosteum were removed from the bone surface. The rib section was cut to the final length and width. The cortical bone was isolated from each rib section and milled into dog bone shaped tension coupons (Figure 9).

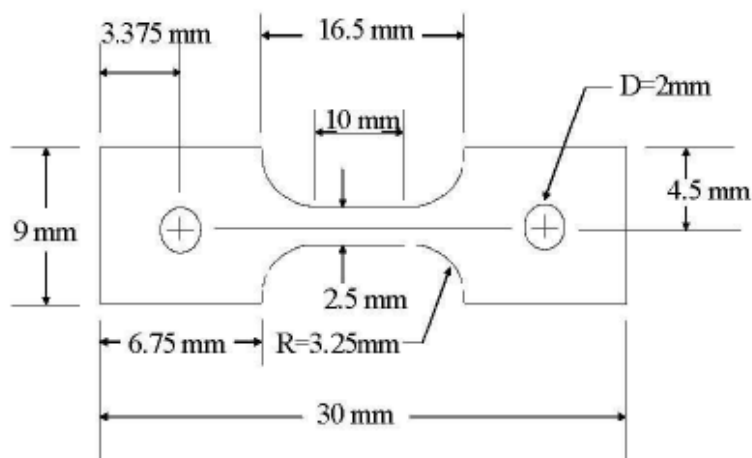


Figure 9: Rib cortical bone 'dog bone' tension specimen dimensions.

### 3.2.2 Testing configuration

A high-rate servo-hydraulic Material Testing System (MTS) machine was used to apply tension loads to failure (Figure 10). The tension tests were run using displacement control. Using MTS and the custom designed slack adapter and grips, the coupons were pulled in tension beyond the point of failure at a target rate of 0.5 strains/s. This strain rate used by Kemper in his test corresponds to the average strain rate resulting from dynamic seat belt loading of the rib cage [3].

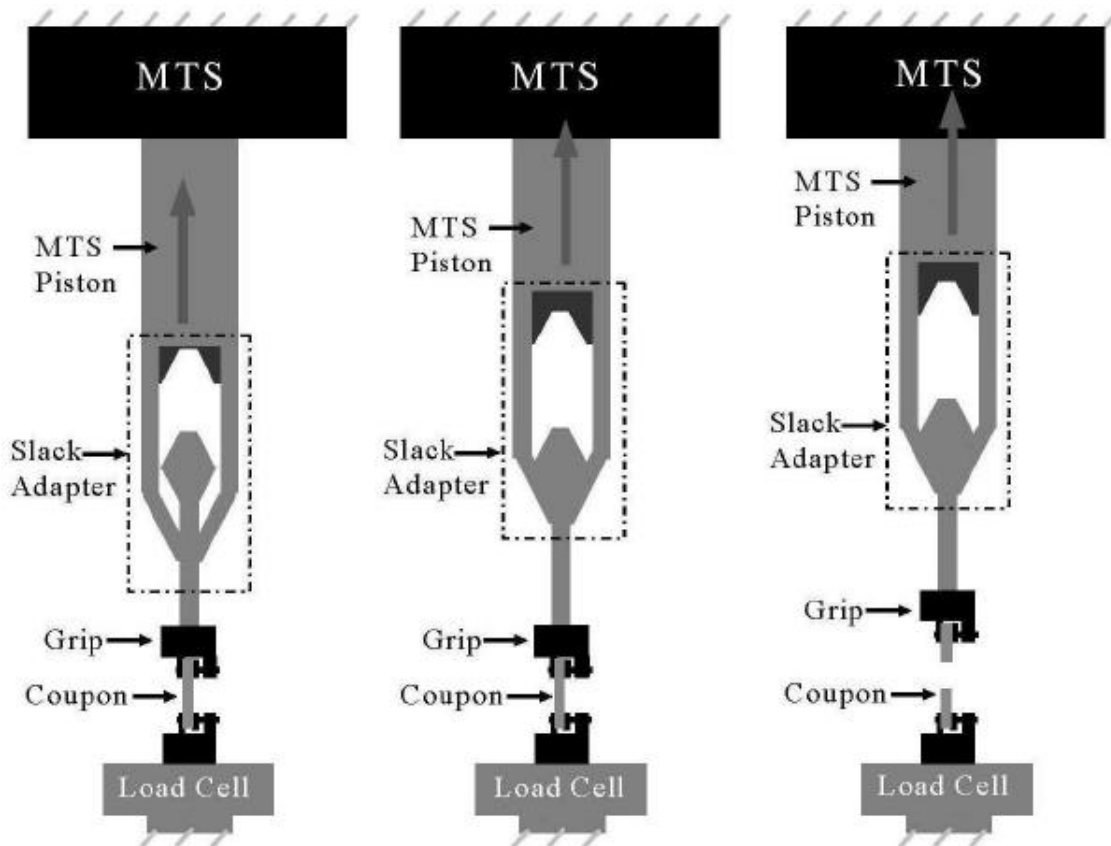


Figure 10: Illustration of the slack adaptor: as the MTS shaft moves upward (left), the slack adaptor is engaged (middle) and pulls the bone coupon to failure (right).

### 3.2.3 Results

Displacement was measured with an extensometer placed directly on the gage length of each coupon (Figure 11).

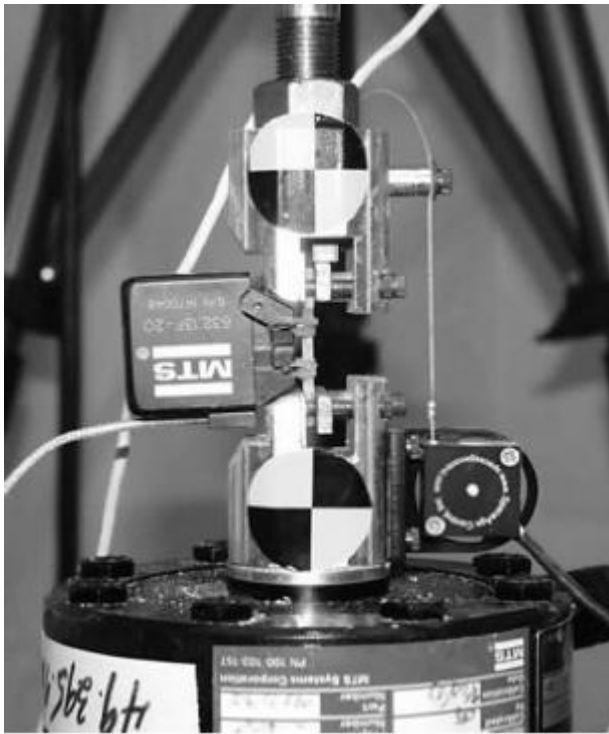


Figure 11: The rib tests utilized the extensometer as the primary strain measurement device and the potentiometer was for redundancy in case of extensometer failure.

The elastic modulus, yield stress, yield strain, ultimate stress, ultimate strain and strain energy density were determined from the resulting stress versus strain curves: Stress was calculated by dividing the force measurement by the cross sectional area of the specimen gage length. Strain was determined dividing the change in length between the extensometer gage arms by the initial length between the extensometer gage arms. The yield point was determined by the intersection of a straight line parallel to the elastic portion of the curve with a 0.2% offset and the stress-strain curve. The modulus of elasticity was defined as the slope between two points, approximately 30% and 70% of the yield point. The strain energy density was calculated by integrating the stress versus strain curve.

The next table shows the values of material properties obtained by Kemper in the tests.

	E [GPa]	$\sigma_{\text{yield}}$ [MPa]	$\varepsilon_{\text{yield}}$ [%]	$\sigma_{\text{ut}}$ [MPa]	$\varepsilon_{\text{ut}}$ [%]
<b>All cadavers</b>	13.9	93.9	0.88	124.2	2.71
<b>All cadavers but 18 year old</b>	14.8	101.9	0.89	129.3	2.27
<b>All male cadavers</b>	12.9	88.2	0.88	120.0	3.06
<b>Older male cadavers (45-67)</b>	14.6	101.3	0.89	134.1	2.38

<b>18 year old male cadaver</b>	9.8	67.2	0.87	106.3	4.24
<b>All female cadavers</b>	15.2	102.7	0.89	129.8	2.23
<b>Older female cadavers (61 and 64)</b>	14.8	101.9	0.89	129.3	2.27

Table 3: Material properties of human rib cortical bone of PMHS used in Kemper's study.

$E$  = Elastic modulus;  $\sigma_{\text{yield}}$  = Yield stress;  $\varepsilon_{\text{yield}}$  = Yield strain;  $\sigma_{\text{ut}}$  = Ultimate stress;  $\varepsilon_{\text{ut}}$  = Ultimate strain.

### 3.3 FEM simulation in Ls-Dyna

The simulation was carried out in the program Ls-Dyna.

#### 3.3.1 Specimen preparation

In the THUMS model, the ribs are simulated as a shell for the cortical bone and as a solid element for the trabecular bone (Figure 12).

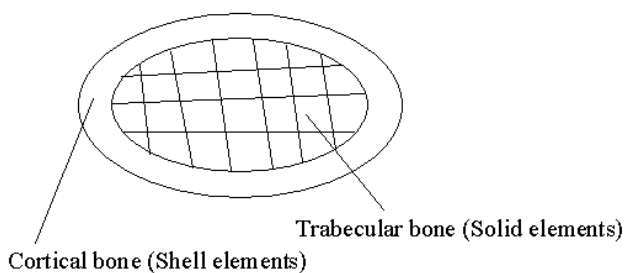


Figure 12: Model of the rib cross section of the THUMS model.

It was decided to analyze a piece of cortical bone (Figure 13).

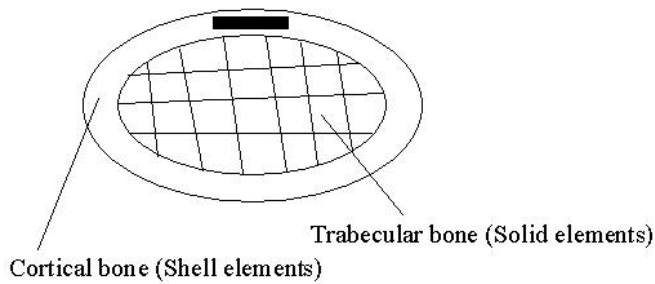


Figure 13: Model of the rib cross section of the THUMS model.

To compare the results with those obtained experimentally by Kemper the FE model has been done identically to the experimental specimen. So, the specimen simulated in FEM has the same 'dog bone' shape and identical measures than the real specimen used by Kemper (2005) (Figure 14).

The specimen has been simulated with shell elements, since it is the cortical bone. The thickness of the specimen is 0.3 mm.

Initial cross section:  $A_0 = 2.5 \text{ mm} \times 0.3 \text{ mm} = 0.75 \text{ mm}^2$

Initial specimen length:  $L_0 = 10 \text{ mm}$ .

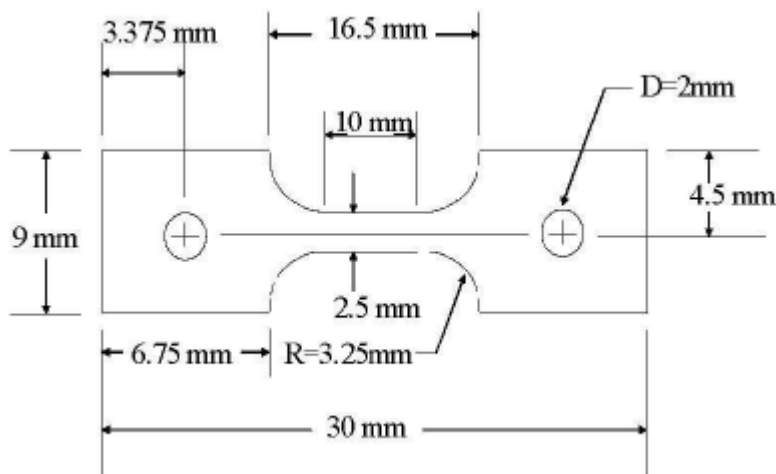


Figure 14: Rib cortical bone 'dog bone' tension specimen dimensions.

### 3.3.2 Testing configuration

A set of nodes in the left side of the specimen was restricted in X, Y and Z both displacement and rotation (Figure 15).

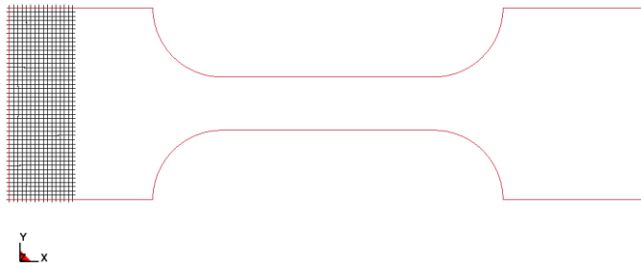


Figure 15: Nodes of the specimen restricted in the simulation.

In a set node in the right side of the specimen was imposed a displacement in X direction (Figure 16). The strain rate is the same imposed by Kemper in his test, a displacement of 0.5 strains/s (5 mm/s).

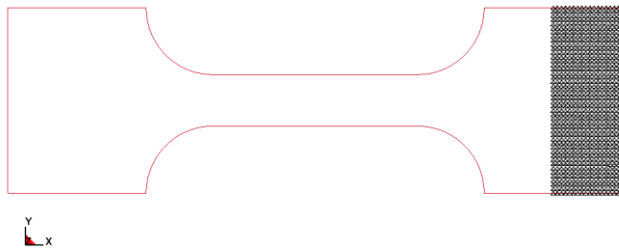


Figure 16: Nodes of the specimen who have an imposed displacement in the simulation.

### 3.3.3 Material properties of human rib cortical bone in FEMs

Table 6 shows the values of material properties of human rib cortical bone used in several FE simulations.

Ref	Author	Model	E [GPa]	$E_t$ [GPa]	$\sigma_{yield}$ [MPa]	$\epsilon_{yield}$ [%]	$\sigma_{ut}$ [MPa]	$\epsilon_{ut}$
[12]	Furusu et al (2001)	THUMS	11.5		73.7	0.64	105.9	2.04 %
[12]	TNO Automotive (2003)	MADYMO FE human model	19.0		73.0	0.38		
[12]	Zhao and Narwanil (2005)	Total Human Body Model	10.2		65.3	0.64		
[12]	Ruan et al (2003)	Full Human Body FEM (Ford)	11.5					

[31]	Z. Li et al (2009)	Simulation of anteroposterior solicitation	11.5	1.15	88	0.02
[13]	Charpail	Simulation of anteroposterior solicitation	13		150	150 10%
	THUMS model		13	0	93.5	150

Table 4: Material properties of human rib cortical bone of different FEM models.

E = Elastic modulus;  $E_t$  = Tangent modulus;  $\sigma_{\text{yield}}$  = Yield stress;  $\varepsilon_{\text{yield}}$  = Yield strain;  $\sigma_{\text{ut}}$  = Ultimate stress;  $\varepsilon_{\text{ut}}$  = Ultimate strain.

### 3.3.4 Material type

The rib cortical bone specimen was simulated with *Piecewise linear plasticity* material. With *Piecewise linear plasticity* material it can be defined an elasto-plastic material with an arbitrary stress versus strain curve and arbitrary strain rate dependency. The stress strain behavior may be treated by a bilinear stress strain curve by defining the tangent modulus. This material includes two attributes: Strain-rate effects and failure criteria.

*Piecewise linear plasticity* material is an isotropic material and it is used for applications as a metal and plastic [32].

Table 7 shows the mechanical properties assumed in THUMS simulation to simulate the cortical bone of rib:

CORTICAL BONE OF RIB	
<b>Material type</b>	Piecewise Linear Plasticity
<b><math>\rho</math> (ton/mm<sup>3</sup>)</b>	2 exp -09
<b>E (MPa)</b>	13000
<b><math>\nu</math></b>	0.3
<b><math>\sigma_y</math> (MPa)</b>	93.5
<b><math>E_t</math> (MPa)</b>	0
<b>Fail</b>	0.018

<b>C</b>	360.70001
<b>P</b>	4.605
$\varepsilon_1$	0
$\varepsilon_2$	0.007154
$\varepsilon_3$	0.0018462
$\sigma_1$ (MPa)	93.5
$\sigma_2$ (MPa)	128
$\sigma_3$ (MPa)	150

Table 5: Simulation parameters of rib specimens

$\rho$  = Mass density;  $E$  = Young's modulus;  $\nu$  = Poisson's ratio;  $\sigma_Y$  = Yield stress;  $E_t$  = Tangent modulus; Fail = Failure flag;  $C$  = Strain rate parameter;  $P$  = Strain rate parameter;  $\varepsilon_1$  = First effective plastic strain value;  $\varepsilon_2$  = Second effective plastic strain value;  $\varepsilon_3$  = Third effective plastic strain value;  $\sigma_1$  = Corresponding yield stress value to  $\varepsilon_1$ ;  $\sigma_2$  = Corresponding yield stress value to  $\varepsilon_2$ ;  $\sigma_3$  = Corresponding yield stress value to  $\varepsilon_3$ .

### 3.3.5 Mesh: Element size

The cortical bone has been simulated like a shell. And it has been simulated using different mesh sizes to choose the most appropriate element size. The two parameters used to choose the element size were convergence and simulation time. The simulation has been done in Ls Dyna with *Piecewise linear plasticity* material type and under-integrated shell elements (integration with one point).

Table 8 shows the parameters of the different simulations.

Mesh size (mm)	Number of elements	Thickness (mm)	Element size/Thickness	Energy at rupture (mJ)	Break time (s)	Ncpu	Time of simulation
<b>2.5</b>	4	0.3	8.33	41.5922	0.086001	1	9 sec
<b>1</b>	25	0.3	3.33	31.5538	0.073801	1	1 min 3 sec
				32.3537	0.074901	2	
<b>0.5</b>	100	0.3	1.67	51.239	0.099801	1	6 min 48 sec
				51.4306	0.099901	2	
<b>0.4</b>	156.25	0.3	1.33	47.8332	0.097101	1	17 min 38 sec
				47.6853	0.099901	2	
<b>0.3</b>	277.78	0.3	1	46.0763	0.119901	1	26 min 17 sec
				45.7188	0.119901	2	
				46.2217	0.119901	4	
<b>0.2</b>	625	0.3	0.67	42.7787	0.090201	1	1 h 4 min 5 sec
				43.5061	0.091201	2	
				43.5024	0.091201	4	

<b>0.1</b>	2500	0.3	0.33	41.6462	0.088101	1	10 h 8 min 16 sec
				42.0234	0.088601	2	
				42.5526	0.089301	4	

*Table 8: Properties of simulation of different meshes.*

Figures 17 and 18 show the energy at rupture and the break time respectively for the different meshes simulated.

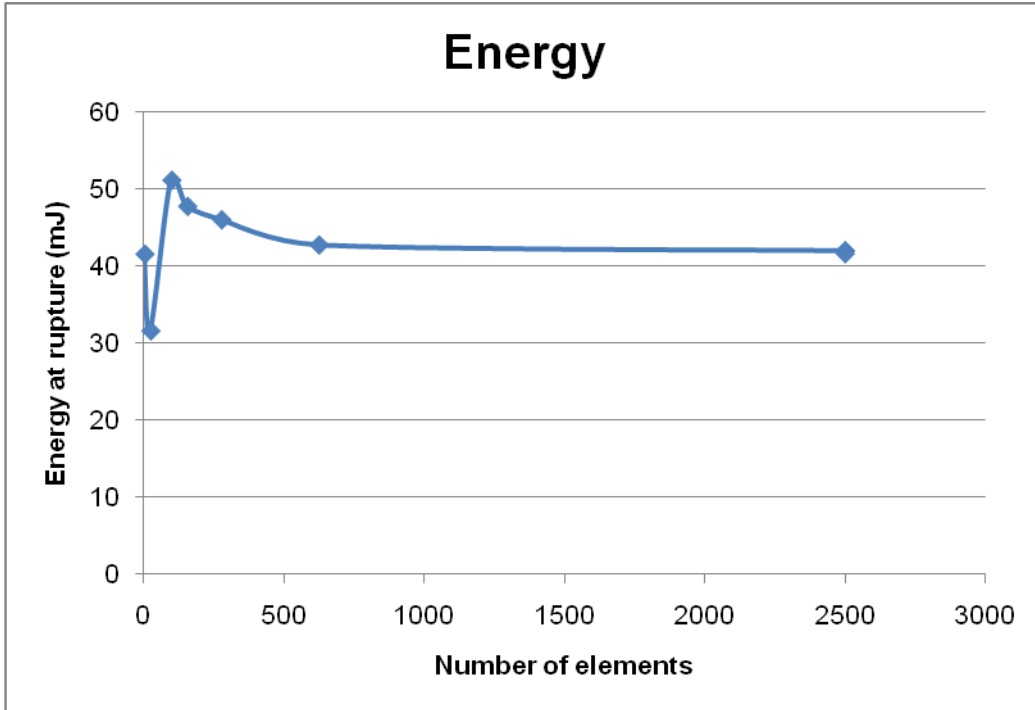


Figure 17: The energy at rupture for different meshes.

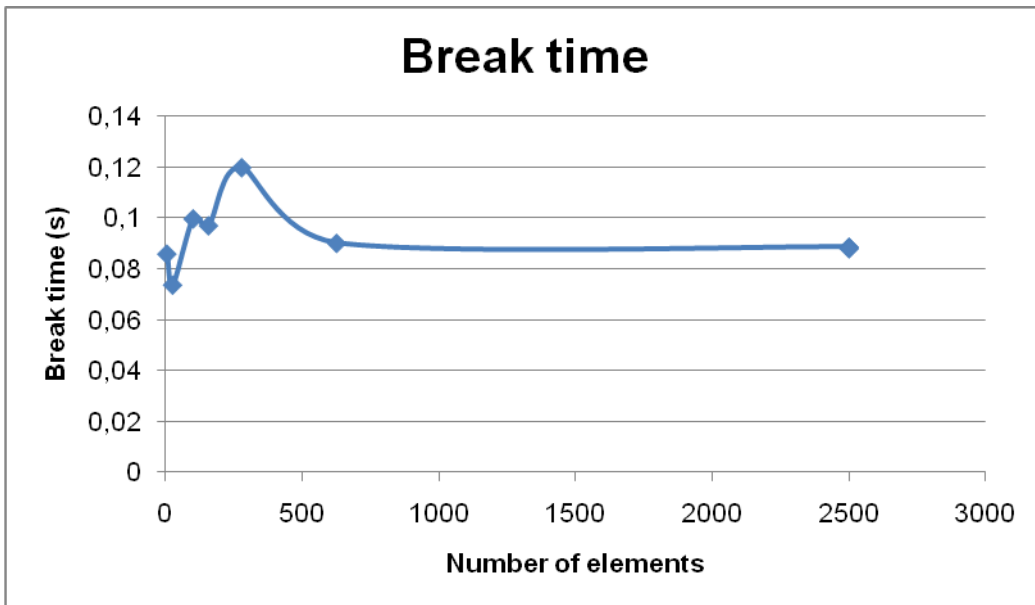
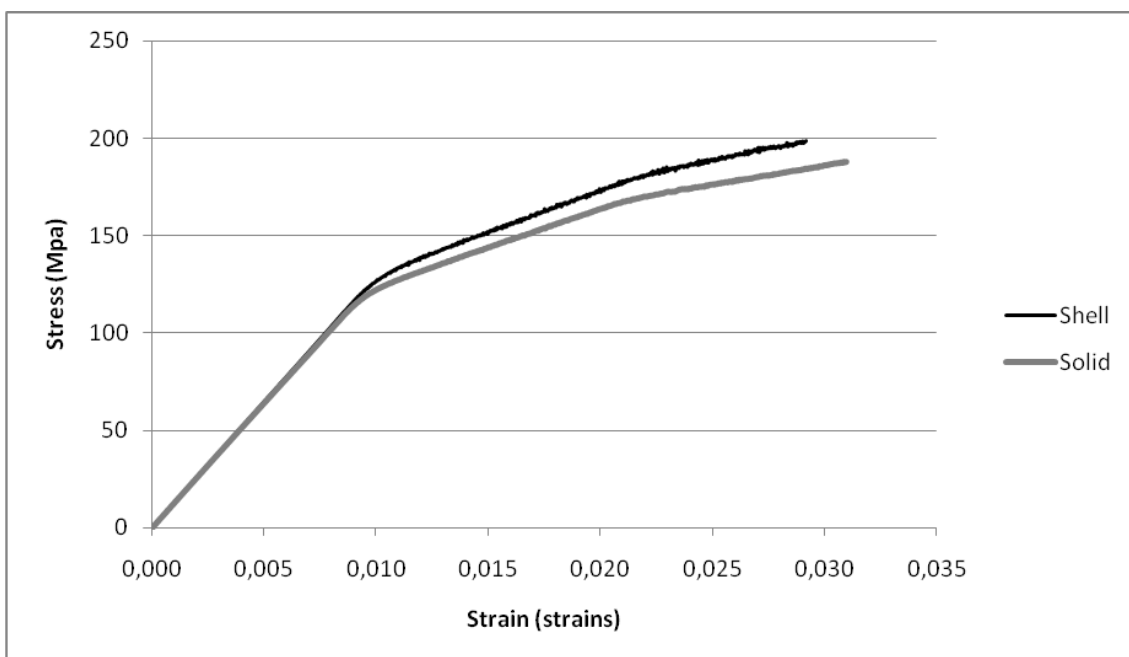


Figure 18: The break time for different meshes.

The breaking energy and the rupture moment are stabilized for an element number of 625 that corresponds with an element size of 0.2 mm. So, the simulation has been done with an element size of 0.2 mm.

As the specimen is simulated like a shell, the element size (0.2 mm x 0.2 mm) is smaller than its thickness (0.3 mm). It was thought that there could be problems due to the size-thickness ratio, so simulations were performed with solid elements and shell elements to see if it influenced. A specimen was simulated using solid elements with an element size of 0.2 mm x 0.2 mm and a thickness of 0.15 mm. Figure 19 shows stress – strain curves of shell and solid specimen taking into account the strain rate effect in the piecewise plasticity material type. The difference may be due to the different ways to calculate the deformation in solid and in shell elements.



*Figure 19: Stress-Strain curve for shell specimen and solid specimen with strain rate parameters.*

Figure 20 shows stress – strain curves of shell and solid specimen without taking into account the strain rate effect. There is no difference between them when the strain rate effects are not considered.

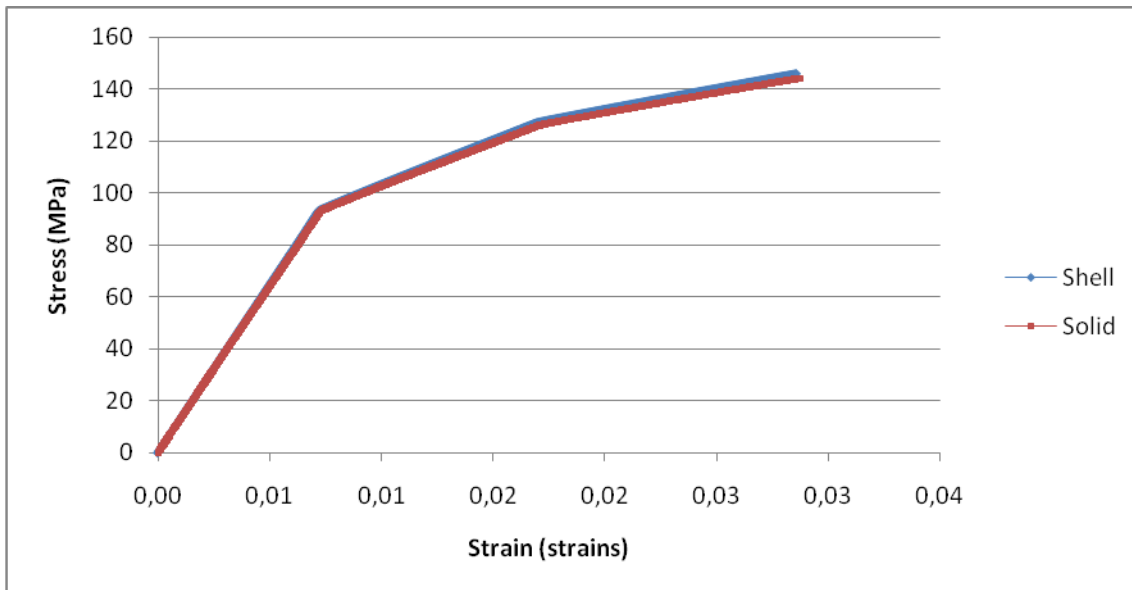


Figure 20: Stress-Strain curve for shell specimen and solid specimen without strain rate parameters.

From these results, it was decided to work with a specimen simulated by shell elements (size of 0.2 mm x 0.2 mm and thickness of 0.3 mm) because its simulation time is approximately the half than this in the solid, and because in the THUMS model the cortical bone is simulated like a shell.

### 3.3.6 Results

The force in axial direction,  $F_x$ , was measured with Ls-Dyna in the restricted set node (nodes in the left) to calculate the stress. Also the displacement of two nodes was measured ( $X_1$  and  $X_2$ ) to calculate the specimen deformation (Figure 21).

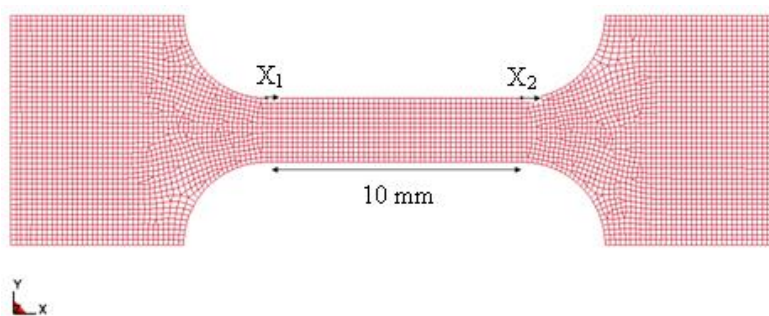


Figure 21: The specimen simulated in Ls Dyna.

Different stress – strain curves are obtained:

Engineering stress – Engineering strain:

$$\sigma_{\text{eng}} = F_x/A_0 \quad \text{Equation 1: Formulation for engineering stress}$$

$$\varepsilon_{\text{eng}} = (X_2 - X_1)/L_0 \quad \text{Equation 2: Formulation for engineering strain}$$

True stress – True strain:

$$\sigma_{\text{true}} = \sigma_{\text{eng}} (1 + \varepsilon_{\text{eng}}) \quad \text{Equation 3: Formulation for true stress}$$

$$\varepsilon_{\text{true}} = \ln (1 + \varepsilon_{\text{eng}}) \quad \text{Equation 4: Formulation for true strain}$$

Effective Stress (Von Misses stress) – Effective Strain:

Given by Ls Dyna.

The effective stress-strain curve was taken for an element in the fracture zone.

Maximum principal stress – Maximum principal strain:

Given by Ls Dyna.

The maximum principal stress-strain curve was taken for an element in the fracture zone.

Figures 22 and 23 show the different curves obtained by all this methods.

The yield stress defined for the cortical bone was 93.5 MPa and taking into account the strain rate parameters defined in THUMS, the yield stress was 115.89 MPa.

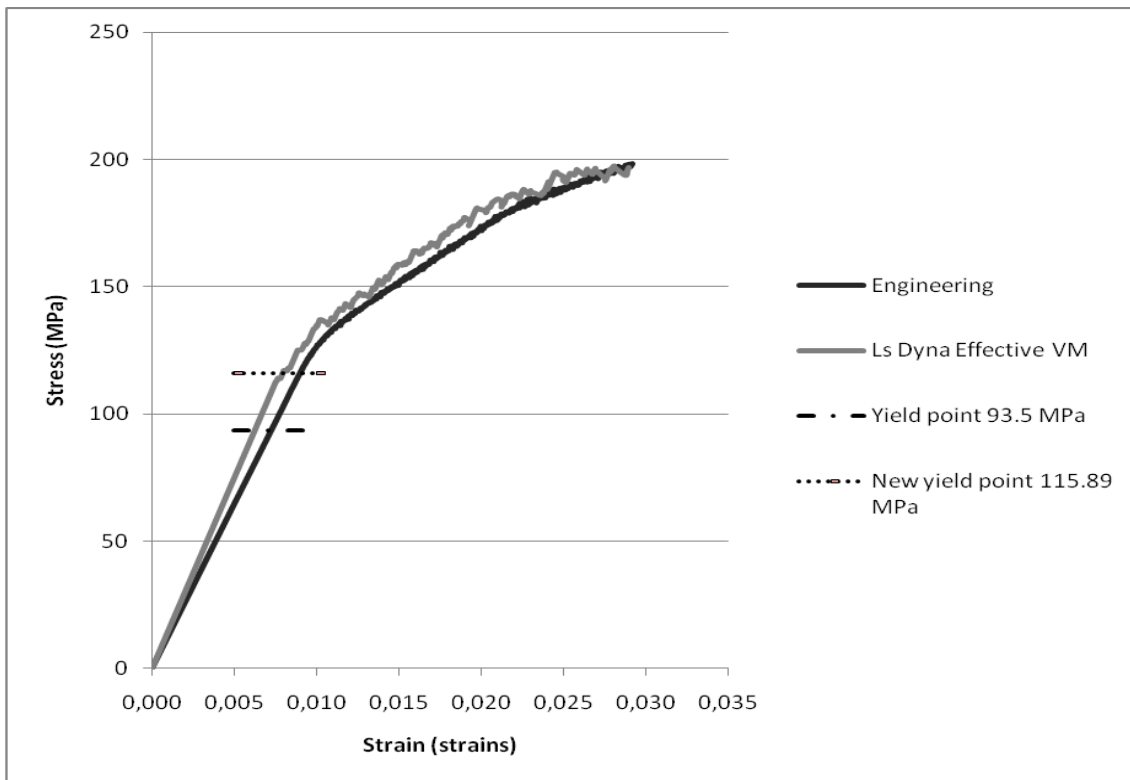


Figure 22: Engineering stress - strain curve and effective stress - strain curve with strain rate factors.

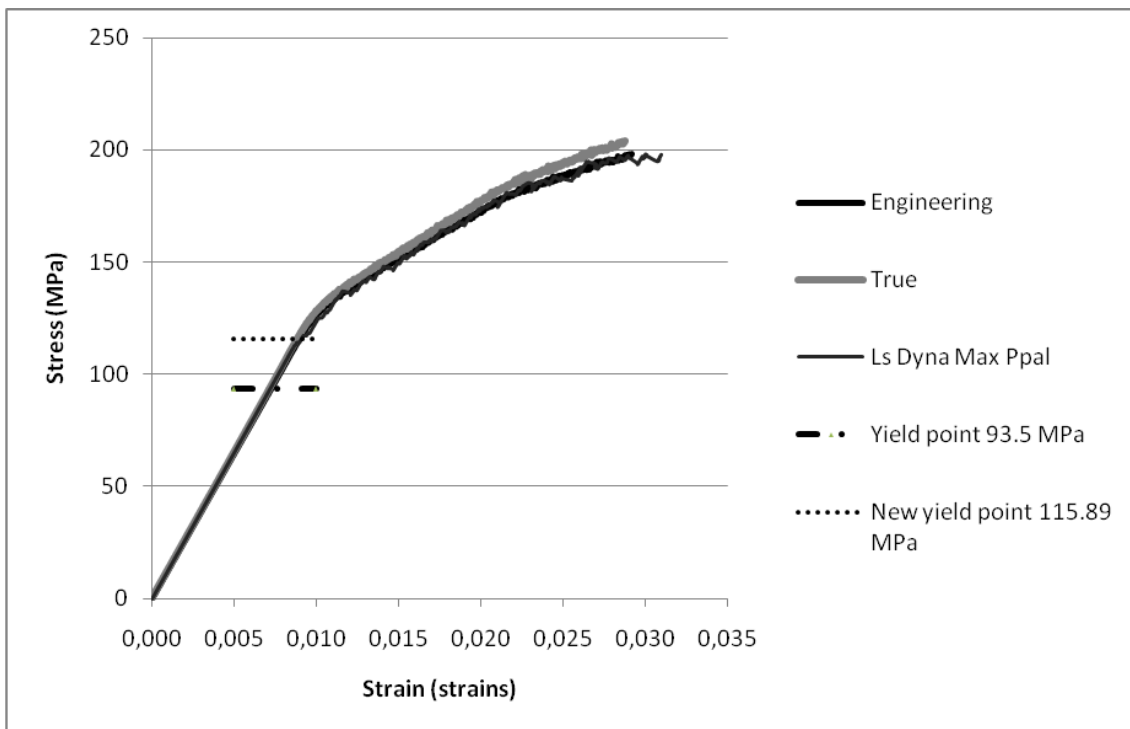


Figure 23: Engineering stress - strain curve, true stress - strain curve and maximum principal stress - strain curve with strain rate factors.

Figures 24 and 25 show stress-strain curves without taking into account the strain rate parameters.

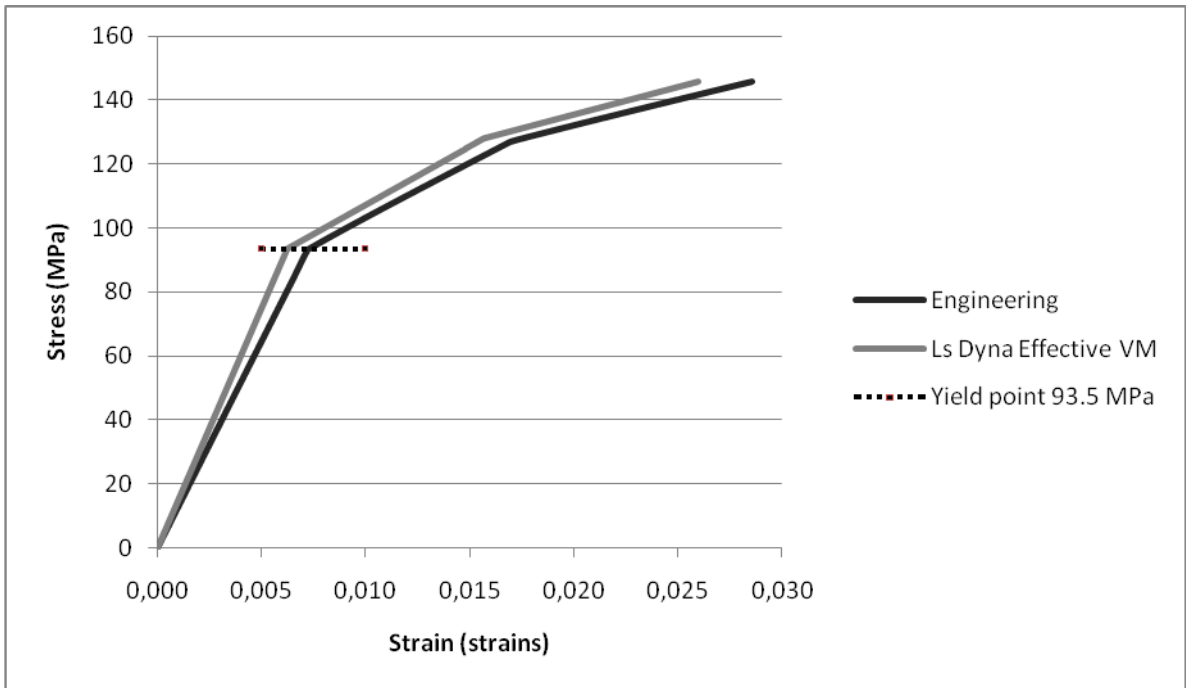


Figure 24: Engineering stress - strain curve and effective stress - strain curve without strain rate factors.

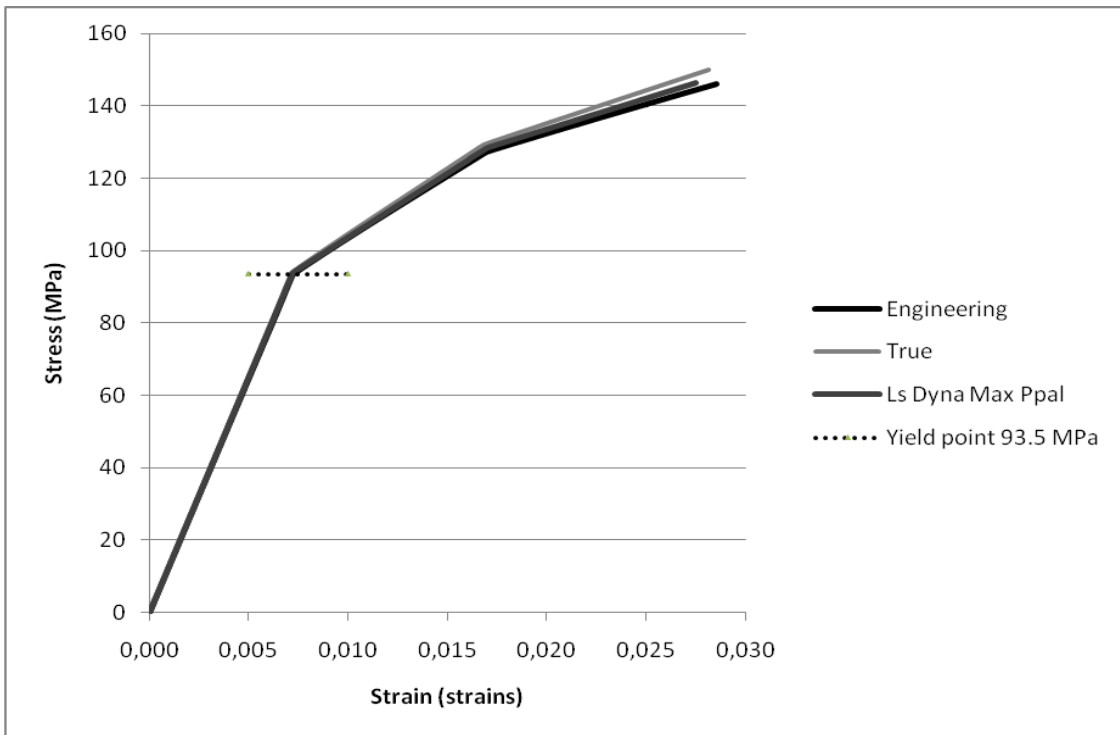


Figure 25: Engineering stress - strain curve, true stress - strain curve and maximum principal stress - strain curve without strain rate factors.

### 3.3.7 Influence of strain rate

Ls Dyna has into account strain rate effects. Specifically, for the *piecewise linear plasticity* the relation is as follows [32]:

$$\beta = 1 + \left(\frac{\dot{\epsilon}}{C}\right)^{1/P}$$

Equation 5: Formulation for  $\beta$  parameter.

$$\sigma_Y = \beta \cdot \sigma_y$$

Equation 6: Formulation for yield stress with the influence of strain rate

Where:

C: Strain rate parameter

P: Strain rate parameter

$\dot{\epsilon}$ : Strain rate

$\sigma_y$ : Yield stress

$\sigma_Y$ : Yield stress with the influence of strain rate

#### **Results with C = 360.70001, P = 4.605**

For THUMS model, with C = 360.70001, P = 4.605 and  $\sigma_y = 93.5$  MPa, the strain rate effect is remarkable in the yield stress (Table 9).

Velocity (mm/s)	Strain rate (strain/s)	$\beta$	$\sigma_Y$ new (MPa)
0	0	1	93.5
0.5	0.05	1.14527027	107.0827699
1	0.1	1.16886785	109.2891442
5	0.5	1.2395146	115.8946154
10	1	1.27842117	119.5323789
50	5	1.39490012	130.4231611

<b>100</b>	10	1.45904738	136.42093
<b>200</b>	20	1.53361467	143.3929717

Table 6: The strain rate effect for  $C = 360.70001$  and  $P = 4.605$

The figures 26, 27 and 28 show the yield stress, the energy versus time and stress-strain curves for different strain rates, respectively.

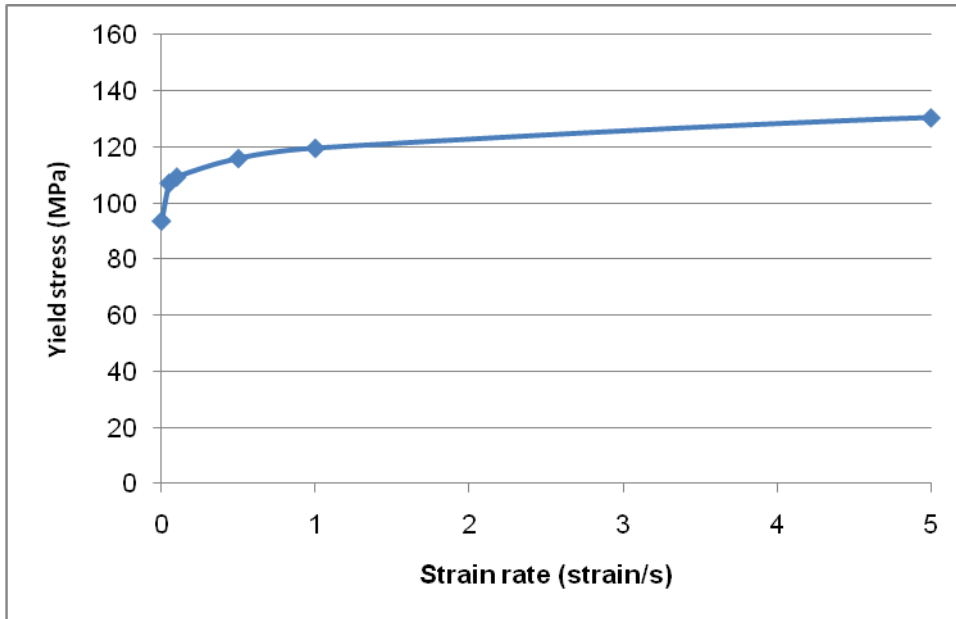


Figure 26: The effect of the strain rate in the yield stress for  $C = 360.70001$  and  $P = 4.605$

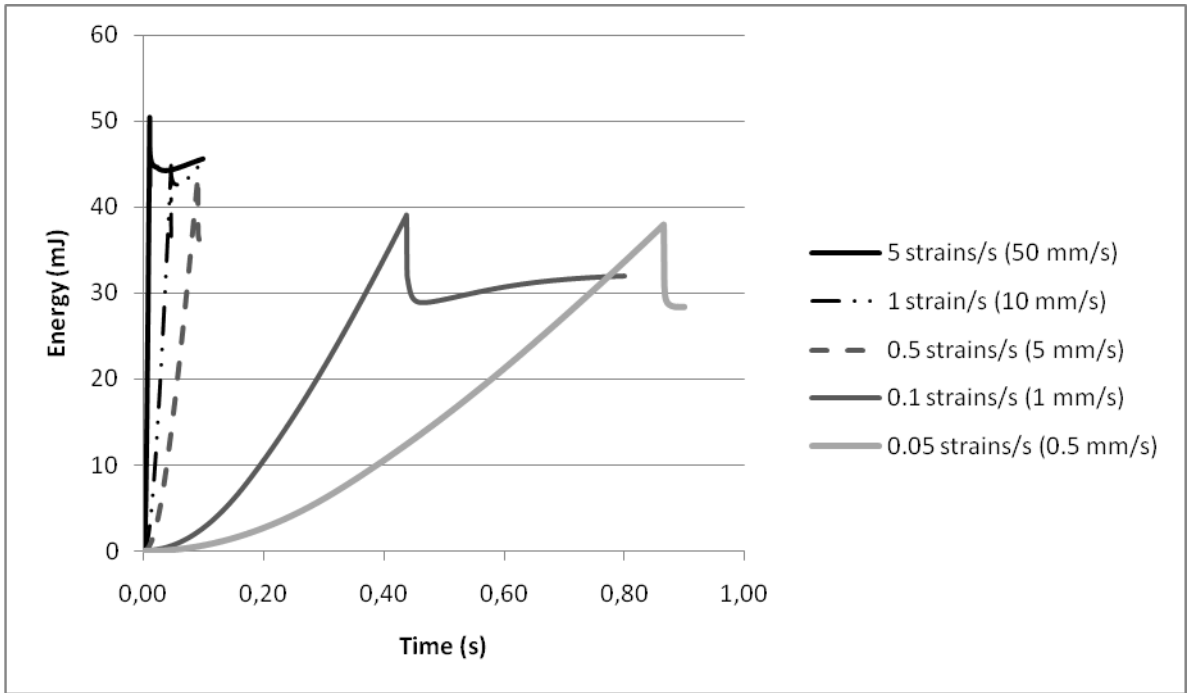


Figure 27: The effect of the strain rate in the energy for  $C = 360.70001$  and  $P = 4.605$

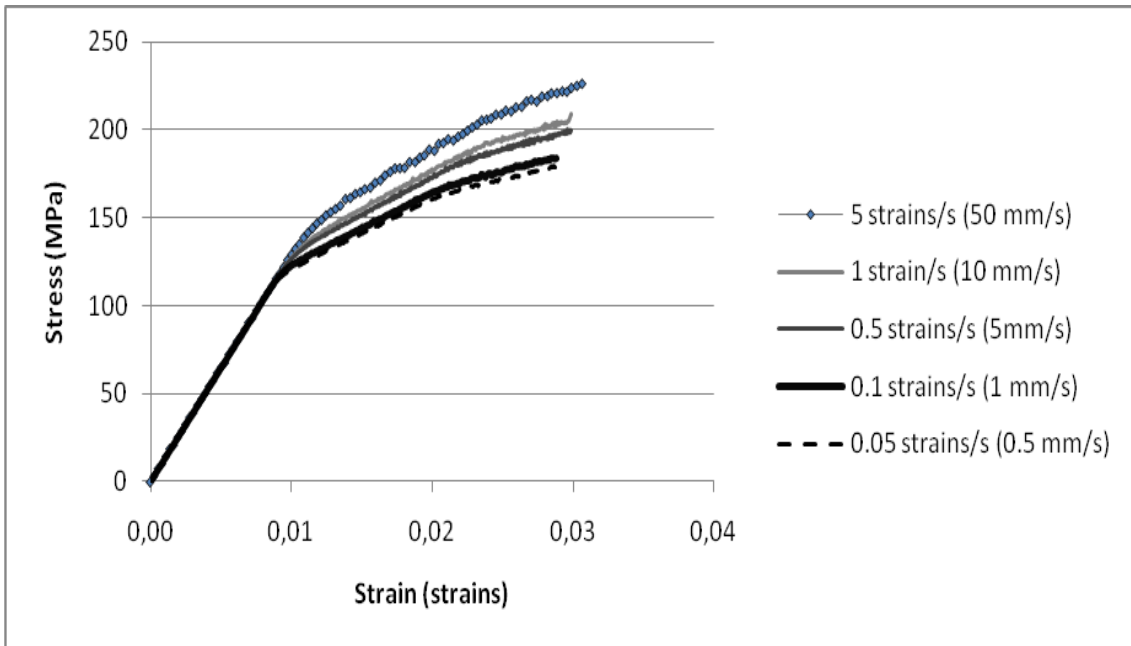


Figure 28: The effect of the strain rate in the stress – strain curve for  $C = 360.70001$  and  $P = 4.605$

Taking into account the effect of the strain rate, the higher is the strain rate, higher is the yield stress and higher is the ultimate stress. This agrees with two tensile test realized with bovine femur and tibia, where the authors concluded that the yield stress increase with the strain rate. And also with several authors who realized tensile test with bovine

and human bones and agrees that the ultimate stress increase with strain rate. However, few authors affirm that ultimate stress decrease or only has a little change with strain rate [30].

### **Results with C = 0 and P = 0**

In Ls Dyna, when C and P parameters are zero, the strain rate effect is not taken into account.

Figures 29 and 30 show respectively the energy versus time and the stress-strain curves for different strain rates without taking into account the strain rate parameters.

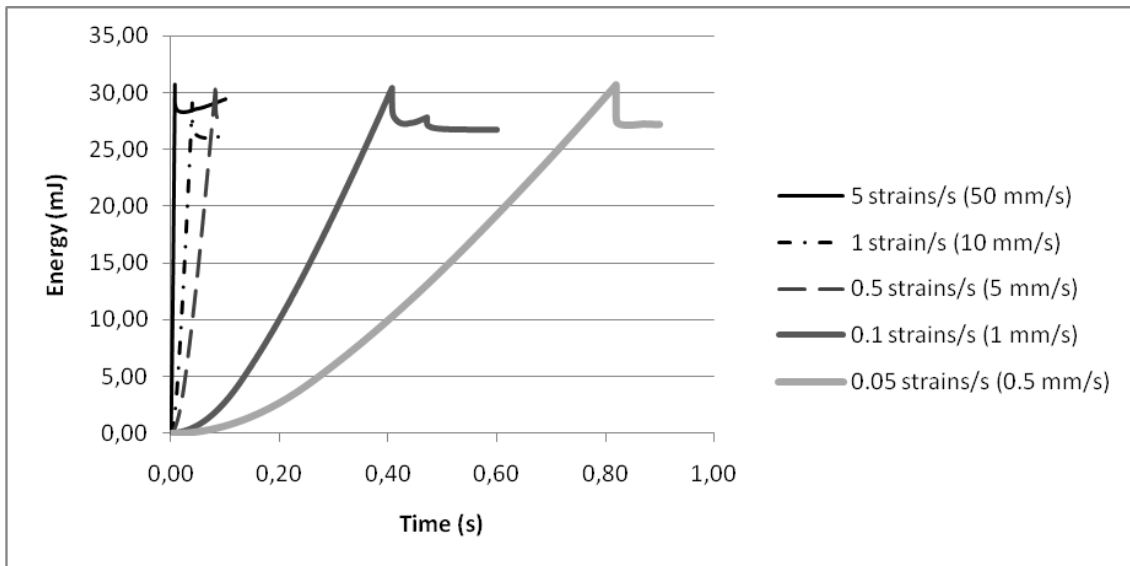


*Figure 29: The energy versus the time for different strain rates without taking into account the strain rate parameters*

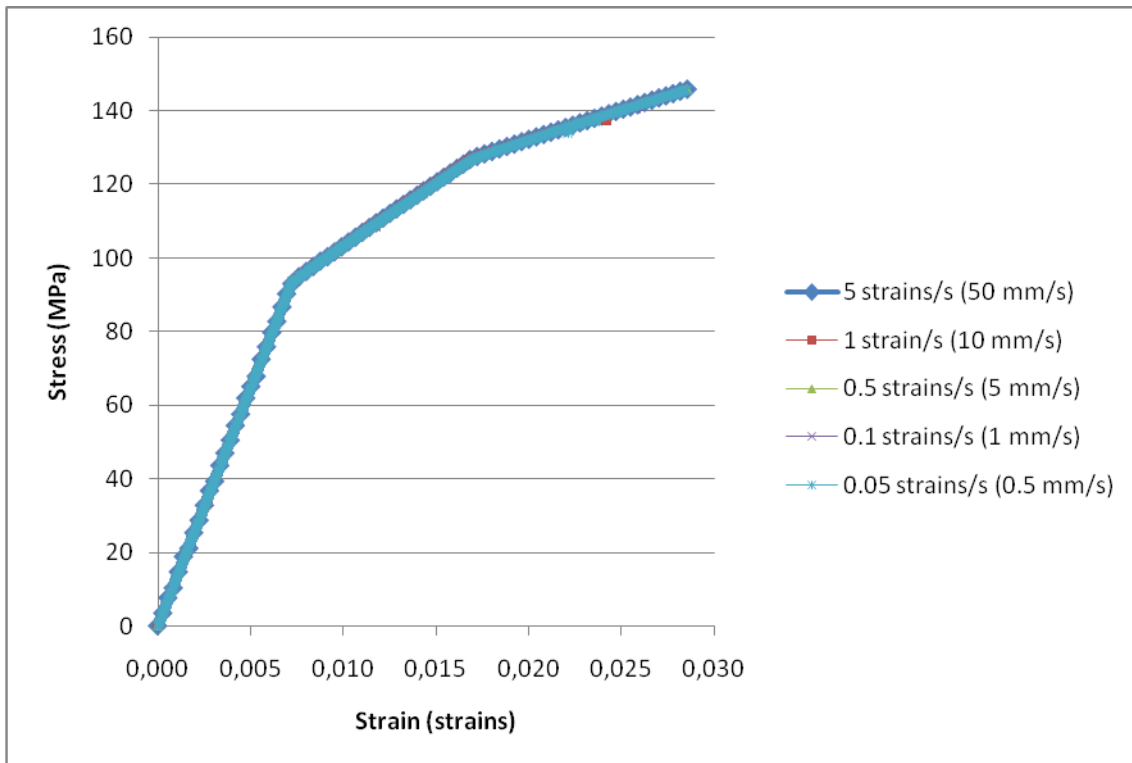


Figure 30: The stress – strain curve for different strain rates without taking into account the strain rate parameters

If the strain rate parameters aren't take into account, the stress – strain curve don't change for different velocities of displacement.

### 3.3.8 Effective plastic strain

The failure effective plastic strain is a parameter to define the piecewise plastic material in LS-Dyna. When any element of the specimen reaches this value, the element disappears and the specimen breaks.

The effective plastic strain in Ls-Dyna is calculated with the Equation 7.

$$\varepsilon_{eff}^p = \int_0^t \left[ \frac{2}{3} \dot{\varepsilon}_{eff}^p \dot{\varepsilon}_{eff}^p \right]^{1/2} dt$$

Equation 7: The effective plastic strain

In THUMS model, the failure effective plastic strain was 0.018 for the rib cortical bone. In the Figure 31 it can be seen the effective plastic strain versus the time.

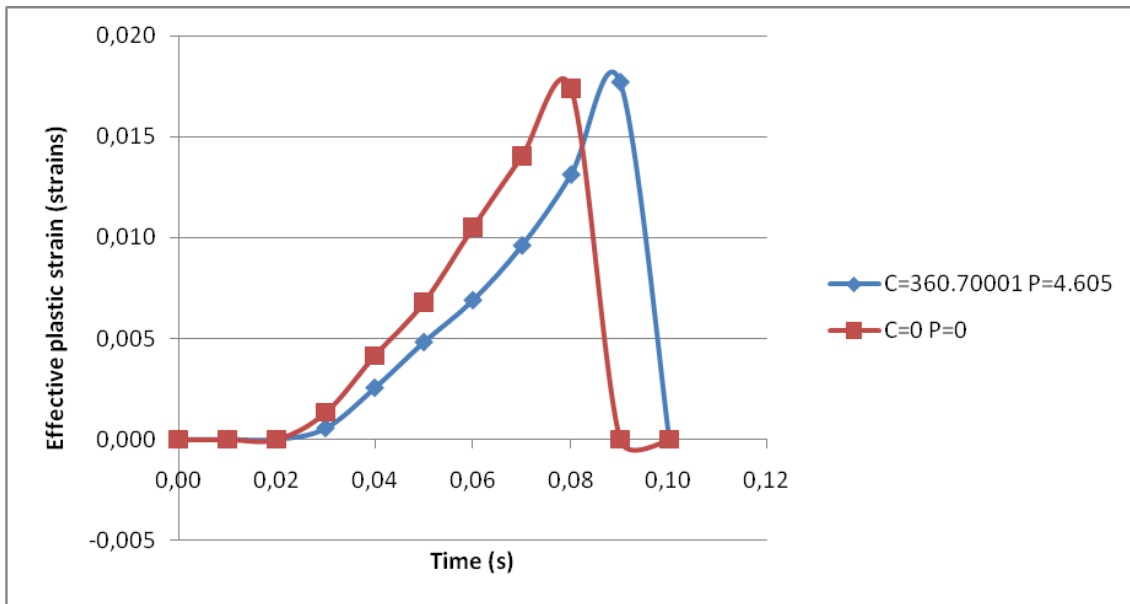


Figure 31: Effective plastic strain versus time

The effective plastic strain over time is different if the strain rate parameters are taken into account or not. If the strain rate parameters are taken into account, at higher strain rate, higher is the yield point, so higher is the elastic zone and it will take longer to break.

But, the effective plastic strain at failure doesn't change, it is the value that it was defined.

### 3.3.9 Comparison with results of Kemper 2005

The simulation of cortical bone of rib, with a shell with element size of 0.2 mm x 0.2 mm, and strain ratio of 0.5 strains/s has been compared with the results obtained experimentally by Kemper. Table 10 shows the mean values of elastic modulus, ultimate stress and ultimate strain obtained by Kemper for all cadavers. With these values, a range was determined.

	E [MPa]	$\sigma_{ut}$ [MPa]	$\varepsilon_{ut}$ [strains]
<b>All cadavers</b>	13960 ± 3760	124.29 ± 32.45	0.02685046 ± 0.01390781

Table 7: The mean value of material properties of all cadavers

Taking into account the strain ratio, with C = 360.70001 and P = 4.605 the result of simulation overestimate the ultimate stress obtained by Kemper. The curves aren't in the range obtained by Kemper (Figure 32).

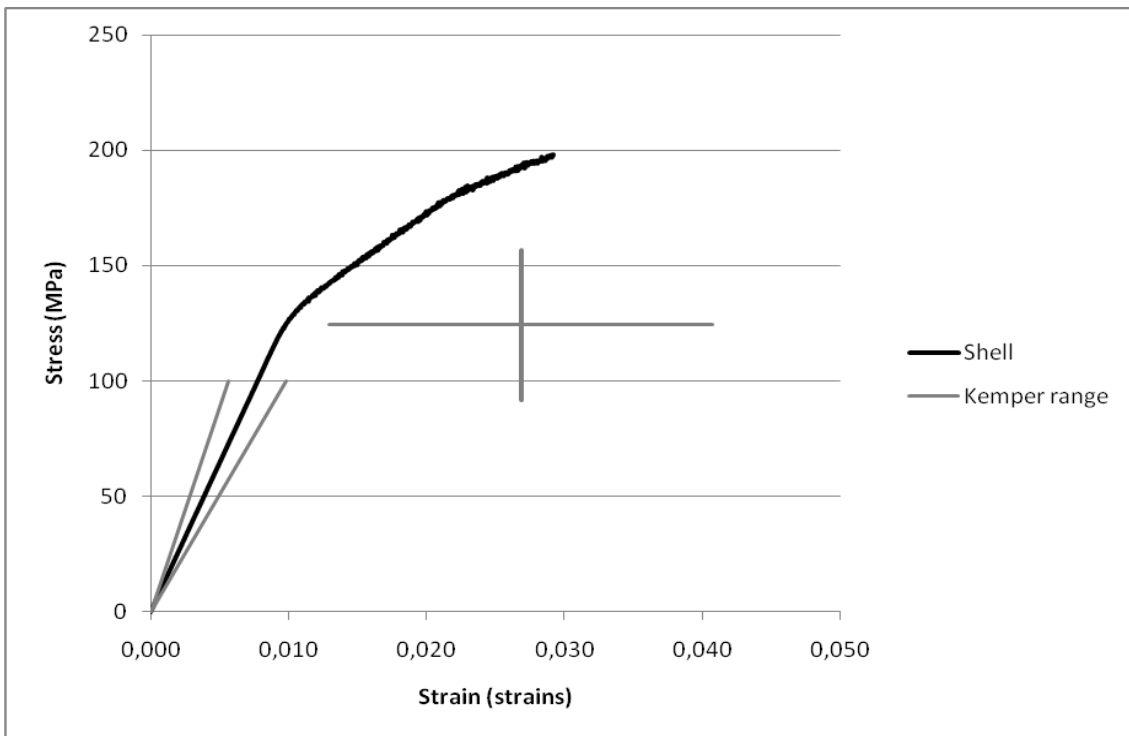


Figure 32: Engineering stress – strain curve with  $C = 360.70001$  and  $P = 4.605$

It can be because of the values de  $C$  and  $P$  are too big. Maybe for a strain rate of 0.5 strain/s it's not necessary to take into account the strain ratio for a dynamic load. It can be seen that without taking into account the influence of the strain ratio, with  $C = 0$  and  $P = 0$ , the curves are similar to these obtained experimentally. They are inside de values given by Kemper (Figure 33).

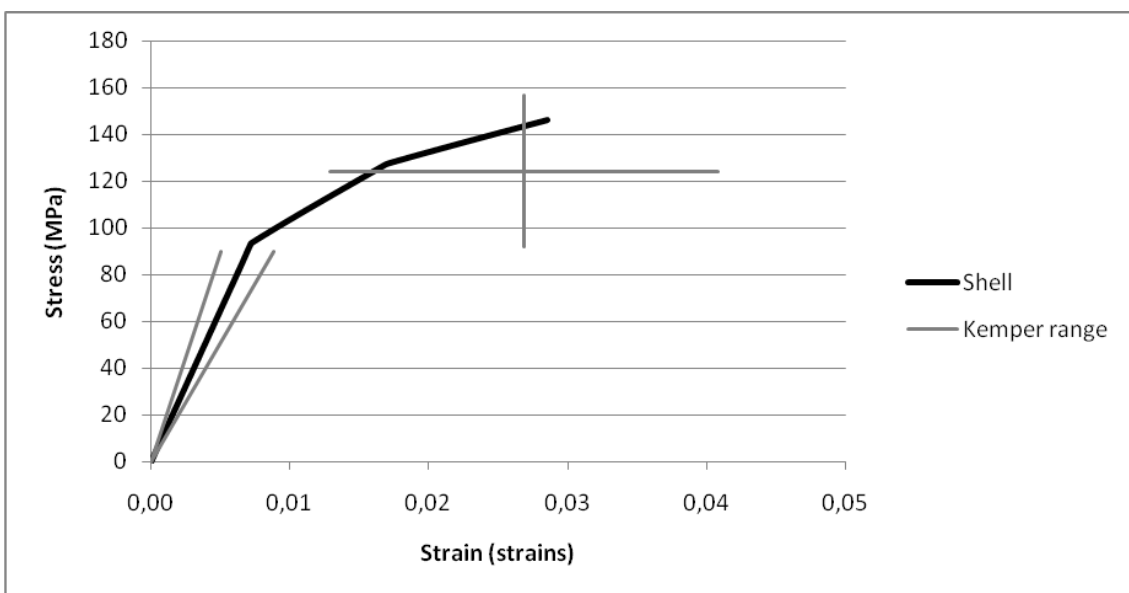


Figure 33: Engineering stress – strain curves with  $C = 0$  and  $P = 0$

The simulation done in Ls Dyna has mechanical values of a man of 30 - 40 years old. The range given by Kemper was done with the average values of six cadavers from 18 to 67 years old. The values are experimental values, but, cannot be affirmed to be significant enough to generalize, because of the low number of PHMS analyzed and the significant differences due to the age.

## 4 Discussion

There is a large need for additional research in mechanical properties of the rib. There are only a few experiments with the cortical bone of the ribs. This small number of experiments may be because only a few years ago has emerged the need to know the mechanical characteristics of bones separately, to model them in FEM.

Data for mechanical properties from experiments with rib bone in literature vary in a large range. The mechanical properties can vary with the type of test, specimen size, individual characteristics (weight, sex, age, skeletal quality, geometry...) and in the same individual, with rib level, rib location and rib section. Not all authors agree with these correlations. It is unclear which parameters influence and which do not in the mechanical properties of the ribs.

In the experiment analyzed, the mechanical properties are of some specific bodies. Although the results are accurate, the values of some specific bodies cannot be generalized for other people. Further, the experiments are usually performed on cadavers of older people, so it can skew the results in mechanical tests.

Another important aspect is the small number of experiments who report the behaviour of bone in the plastic zone and the rupture zone. There are few experiments to define the parameters C and P in this case.

Kemper performed the tensile test only a concrete strain rate. So, it is difficult to evaluate the dependency between the behavior in the plastic region of the bone and the strain rate. It is not found any experiment involving the cortical bone at different strain rates in order to assess the dependence of the plastic region and the strain rate.

The test was simulated with the initial material properties defined for THUMS, and it was seen that the results overestimate the values obtained by Kemper. The test was simulated again without taking into account the parameters of strain rate. And the results were more similar to these obtained by Kemper. Without taking into account the parameters of strain rate, the results are more similar to the real values, however, in this way it fails to consider the bone as a viscoelastic material.

## 5 Future work

For a better analysis of the mechanical behavior of rib and rupture threshold, it can perform a test of the entire rib (cortical and trabecular bone, and the geometry of the entire rib). It would be nice to simulate an anteroposterior compression test, to be closer to the loads to the rib subjects in a frontal impact. The results can be compared with the experiment realized by Charpail et al.: *Characterization of PMHS ribs: A new test methodology* [3] in which they break the ribs of five cadavers by anteroposterior compression test as in Figure 34.

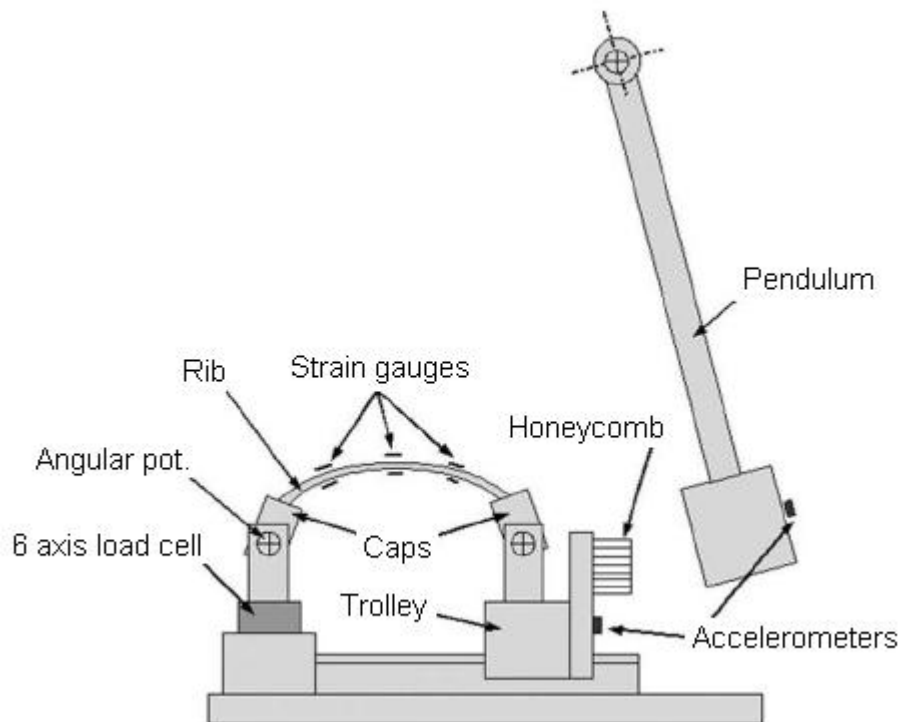


Figure 34: Test rig used by Charpail et al [3].

## 6 Conclusion

- The internal energy and the rupture moment are stabilized for a shell element size of 0.2 mm x 0.2 mm.
- Shell element of 0.2 mm x 0.2 mm with a thickness of 0.3 mm and two layers of solid elements of 0.2 mm x 0.2 mm with a thickness of 0.15 mm have the same stress-strain curve if the strain rate parameters are not taken into account. So, if the strain rate parameters are not taking into account, the ratio element size/thickness for a shell element used in these simulations does not affect the results.
- Taking into account the effect of the strain rate, with the Ls Dyna definition included in the material Piecewise linear plasticity, the higher is the strain rate, higher is the yield stress.
- If the strain rate parameters aren't taken into account, the stress-strain curve don't change for different velocities of displacement.
- The effective plastic strain over time is different if the strain rate parameters are taken into account or not. If the strain rate parameters are taken into account, it will take longer to break.
- Taking into account the strain ratio, with  $C = 360.70001$  and  $P = 4.605$ , the stress-strain curves aren't in the range obtained experimentally by Kemper.
- Without taking into account the influence of the strain ratio, with  $C = 0$  and  $P = 0$ , stress-strain curves are similar to these obtained experimentally. They are inside the values obtained by Kemper.

## 7 References

- [1] Beaupied H., Lespessailles E., Benhamou C. (2006): Evaluation of macrostructural bone biomechanics. *Joint Bone Spine* 74 (2007) pp 233 – 239.
- [2] J. W. Melvin (1993): Fracture mechanics of bone. *Journal of Biomechanical Engineering* November 1993, Vol. 115 / 549.
- [3] Kemper A., McNally C., Kennedy E., Manoogian S. et al (2005): Material Properties of Human Rib Cortical Bone from Dynamic Tension Coupon Testing. *Stapp Car Crash Journal*. November 2005. Vol. 49. pp. 199 – 230.
- [4] Charpail E., Trosseille X., Petit P., Laporte S. et al (2005): Characterization of PMHS ribs: A new test methodology. *Stapp Car Crash Journal*. November 2005. Vol. 49. pp 183 - 198.
- [5] Kent R., Forman J., Evans J. et al (2006): Thoracic Response of Belted PMHS, the Hybrid III, and the THOR-NT Mid-Sized Male Surrogates in Low Speed, Frontal Crashes. *Stapp Car Crash Journal*. November 2006. Vol. 50. pp 191 – 215.
- [6] Flagel B., Luchette F., Esposito T., Santaniello J. et al (2005): Half-a-dozen ribs: The breakpoint for mortality. 62<sup>nd</sup> Annual Meeting of the Central Surgical Association, Tucson, Arizona. March 2005.
- [7] Kemper A.R., McNally C., Pullins C., Freeman L., Duma S. et al (2007): The Biomechanics of Human Ribs: Material and Structural Properties from Dynamic Tension and Bending Tests. *Stapp Car Crash Journal*. October 2007. Vol. 51 pp. 235-273.
- [8] Pipkorn B., Halldin P., Jakobsson L. et al (2008): Mathematical Human Body Models in Side Impacts – A Validation Study with Particular Emphasis on the Torso and Shoulder and their Influence on Head and Neck Motion. IRCOBI Conference – Bern (Switzerland). September 2008
- [9] Users' Guide of Computational Human Model THUMS (Total HUMAN Model for Safety). AM50 Occupant Model: Version 3.0-080225. March 2008. Toyota Central R&D Labs., Inc.
- [10] Murakami D., Kobayashi S., Torigaki T., Kent R. (2006): Finite element analysis of hard and soft tissue contributions to thoracic response: Sensitivity analysis of fluctuations in boundary conditions. *Stapp Car Crash Journal*. November 2006. Vol. 50. pp 169 – 189.
- [11] Alvin S. Hyde, Ph. D., M.D.: *Crash injuries: How and why they happen*.
- [12] Schmitt K., Niederer P., Walz F. (2004): *Trauma Biomechanics: Introduction to Accidental Injury*.

- [13] Charpail, Estelle (2006): Analyse du comportement mécanique des côtes humaines en dynamique. Thèse à l'École Nationale Supérieure d'Arts et Métiers, Paris.
- [14] Ordaka J., Meijer R., Rooij L. et al (2007): Validation of a Finite Element Human Model for Prediction of Rib Fractures. SAE 2007-01-1161. Detroit, Michigan.
- [15] Turner C., Takaro Y., Tsui T., Pharr G. et al (1999): The elastic properties of trabecular and cortical bone tissues are similar: results from two microscopic measurement techniques. *Journal of Biomechanics* 32 (1999) pp 437-441.
- [16] Kimpara H., Iwamoto M. et al (2006): Effect of Assumed Stiffness and Mass Density on the Impact Response of the Human Chest Using a Three-Dimensional FE Model of the Human Body. *Journal of Biomechanical Engineering* 772 / Vol. 128, October 2006.
- [17] Mercer C., He M.Y., Evans A.G. et al (2006): Mechanisms governing the inelastic deformation of cortical bone and application to trabecular bone. *Acta Biomaterialia* 2 (2006) pp. 59 – 68.
- [18] Vashishth D, Tanner KE, Bonfield W. (2001): Fatigue of cortical bone under combined axial-torsional loading. *J. Orthopaedic Research* 2001.19:414 - 20.
- [19] Yoganandan N. and Pintar F.A. (1998): Biomechanics of Human Thoracic Ribs. *ASME* 100 / Vol. 120, February 1998.
- [20] M. P. Akhter, U. T. Iwaniec, M. A. Covey, D. M. Cullen, D. B. Kimmel, R. R. Recker (1999): Genetic Variations in Bone Density, Histomorphometry, and Strength in Mice.
- [21] Lind P.M., Larsson S. and Orberg J.: Torsional Testing and Peripheral Quantitative Computed Tomography in Rat Humerus
- [22] Kimpara H., Iwamoto M., Miki K. et al (2003): Biomechanical properties of the male and female chest subjected to frontal and lateral impacts. *IRCOBI Conference – Lisbon (Portugal)*. September 2003
- [23] Stitzel J., Cornier J. et al (2003): Defining Regional Variation in the Material Properties of Human Rib Cortical Bone and Its Effect on Fracture Prediction. *Stapp Car Crash Journal*. October 2003. Vol. 47. pp 243 – 265.
- [24] Kaneko TS, Pejčić MR, Tehranzadeh J, Keyak JH.: Relationships between material properties and CT scan data of cortical bone with and without metastatic lesions. *Med Eng Phys* 2003;25:445 - 54.
- [25] Goss P.E., Pritzker K.P.H., Mendes M. et al: The steroidal aromatase inhibitor exemestane prevents bone loss in ovariectomized rats.
- [26] Neil Dong X., Guo E.: The dependence of transversely isotropic elasticity of human femoral cortical bone on porosity.
- [27] Pithioux M., Subi D., Chabrand P.: Comparison of compact bone failure under two different loading rates: experimental and modelling approaches.

[28] Bessho M., Ohnishi I., Matsuyama J. et al (2007): Prediction of strength and strain of the proximal femur by a CT-based finite element method. *Journal of Biomechanics* 40 (2007). pp 1745 - 1753

[29] Arregui-Dalmases C., Del Pozo E., Duprey S., López-Valdes J., Kent R. et al (2008): A parametric study of hard tissue injury prediction using finite elements: Consideration of geometric complexity, sub-failure material properties, CT-Thresholding, and element characteristics. IRCOBI Conference – Bern (Switzerland) – September 2008

[30] Hansen U., Zioupos P., Simpson R., Currey J. et al: The Effect of Strain Rate on the Mechanical Properties of Human Cortical Bone. *Journal of Biomechanical Engineering*. February 2008. Vol. 130 / 011011-1.

[31] Zuoping Li, W.Kinding M., Kent R. et al (2009): Rib fractures under anterior-posterior dynamic loads: Experimental and finite-element study. *Journal of Biomechanics*.

[32] Ls Dyna Tutorial

## 8 Appendix

### 8.1 Stress - strain curves of cadaver 2 (male of 45 years old) and cadaver 6 (male of 18 years old) obtained by Kemper

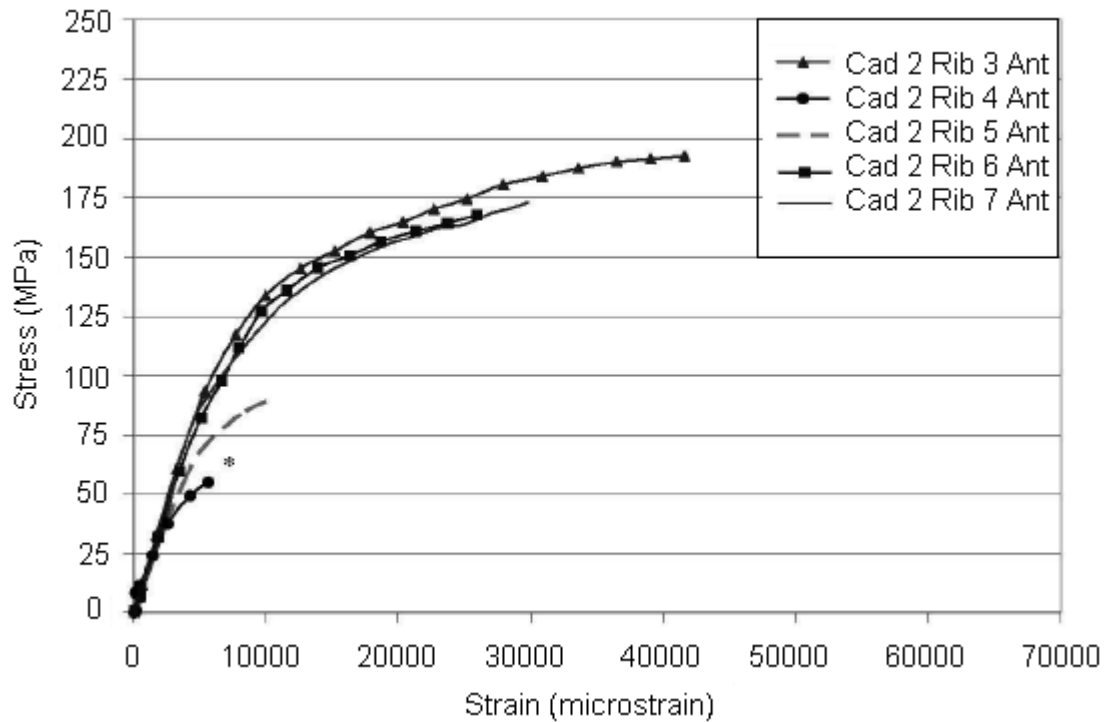


Figure 35: Cadaver 2 anterior section stress versus strain plot

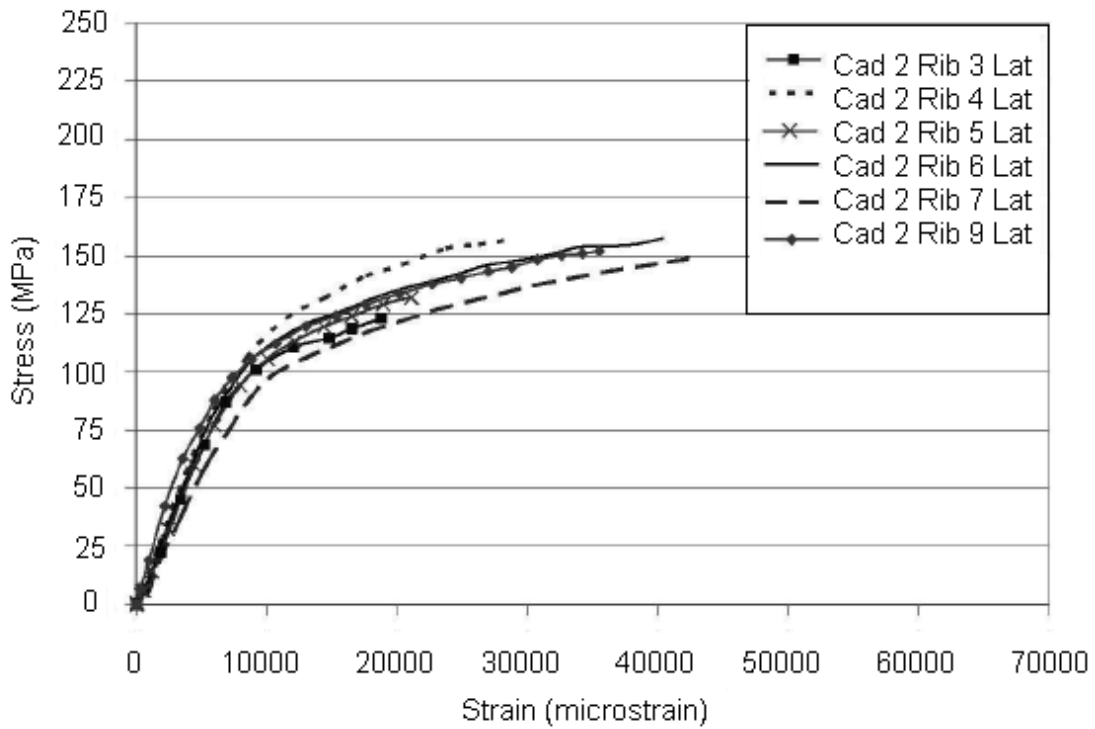


Figure 36: Cadaver 2 lateral section stress versus strain plot

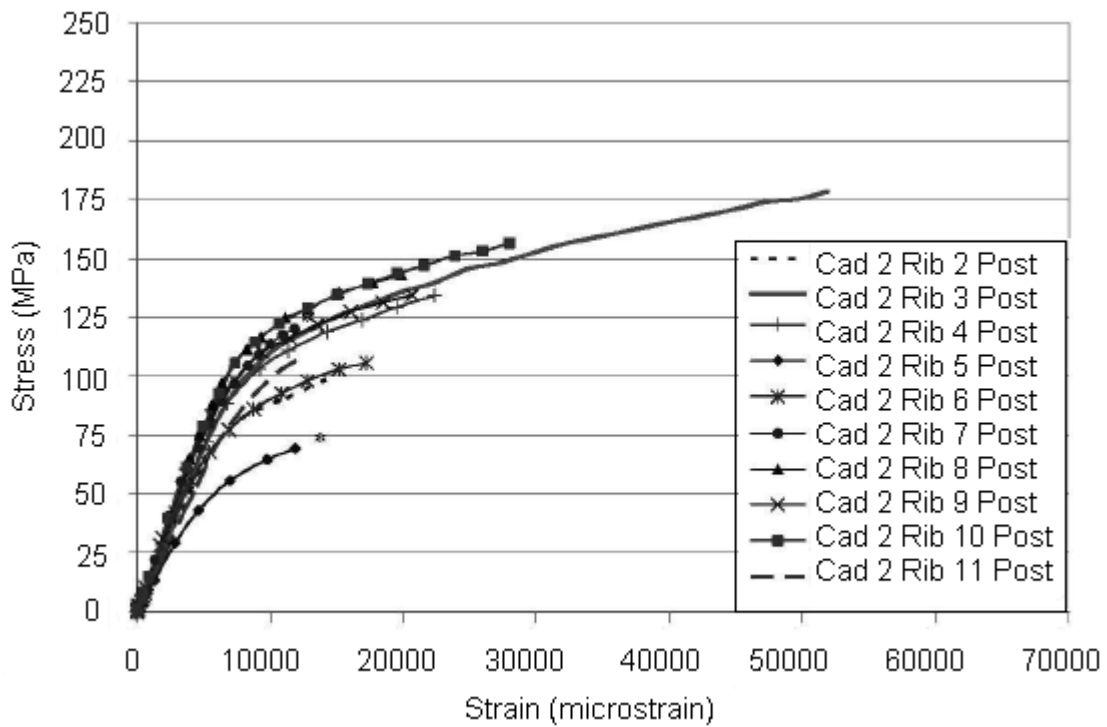


Figure 37: Cadaver 2 posterior section stress versus strain plot

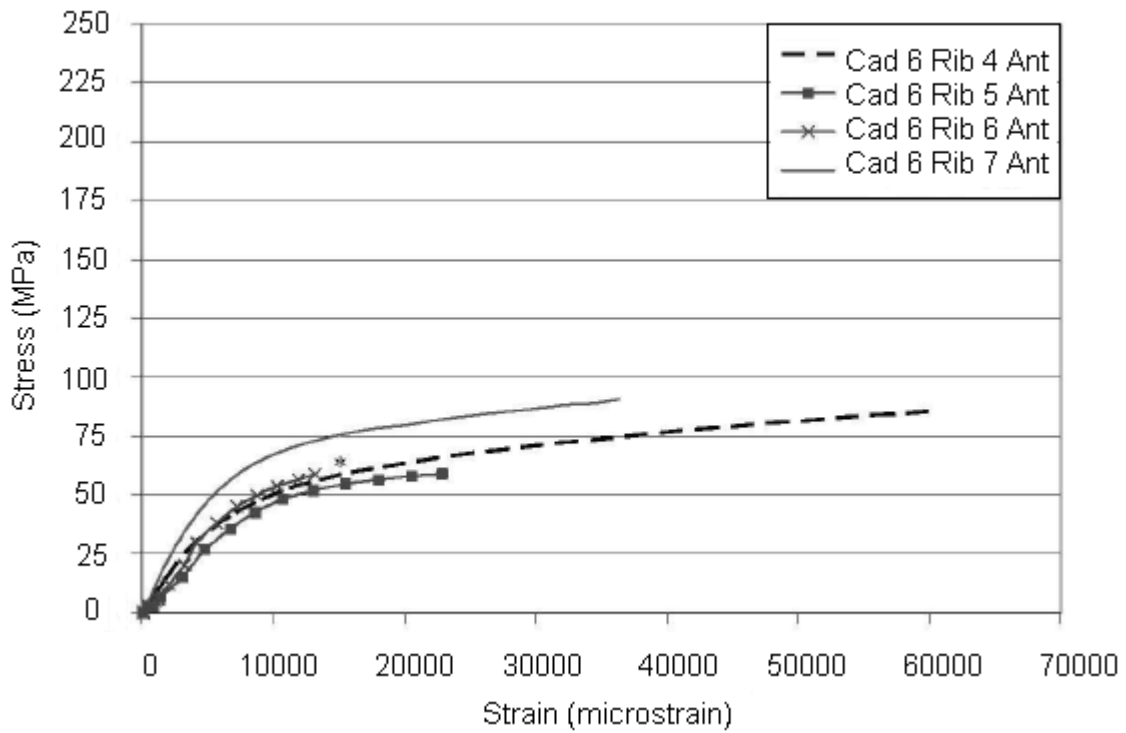


Figure 38: Cadaver 6 anterior section stress versus strain plot

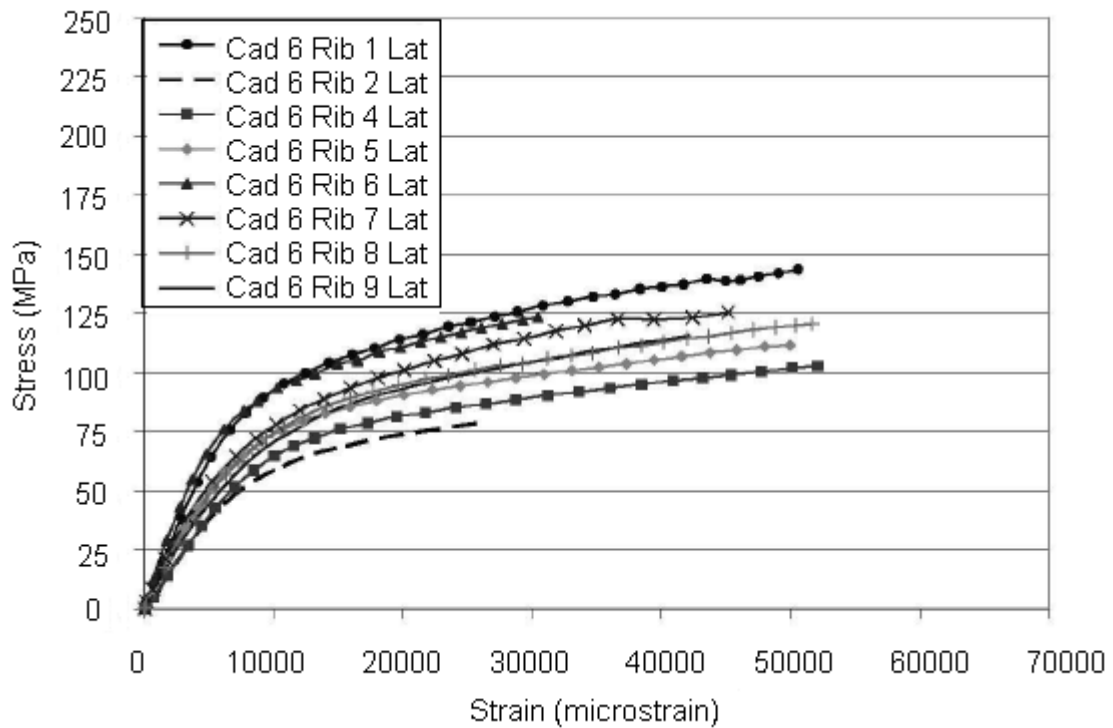


Figure 39: Cadaver 6 lateral section stress versus strain plot

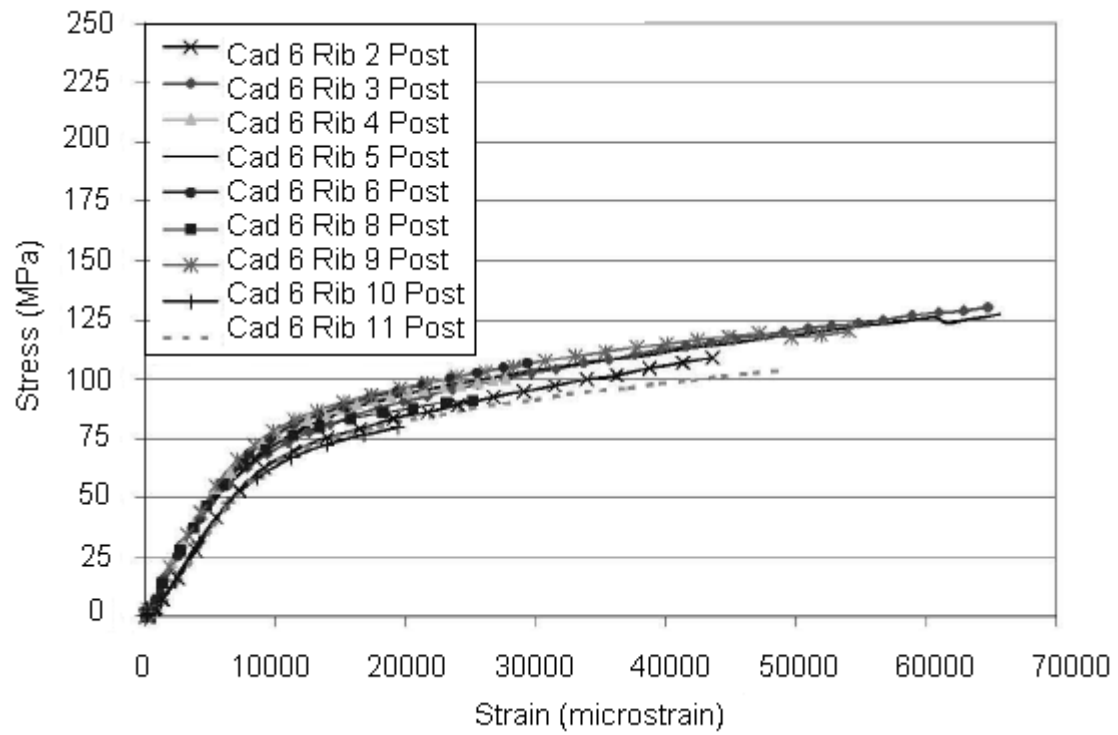
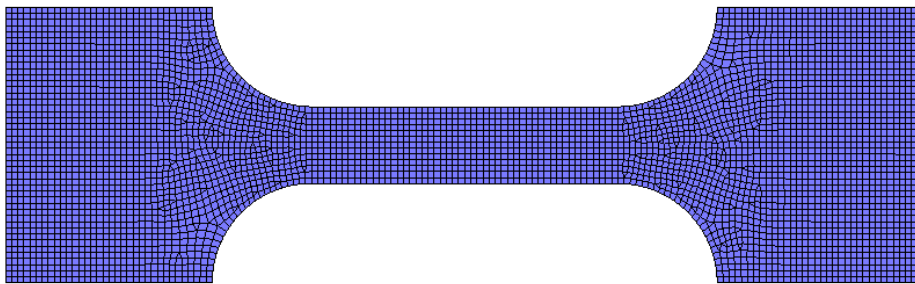


Figure 40: Cadaver 6 posterior section stress versus strain plot

## 8.2 Simulation of tensile test. Shell element of 0.2 mm and strain rate of 0.5 strains/s.

### LS-DYNA KEYWORD DECK BY LS-PREPOST

Time = 0  
Contours of Effective Plastic Strain  
max ipt. value  
min=0, at elem# 20076  
max=0, at elem# 20076



Fringe Levels

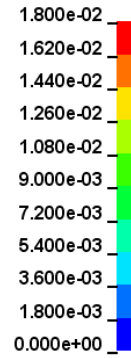
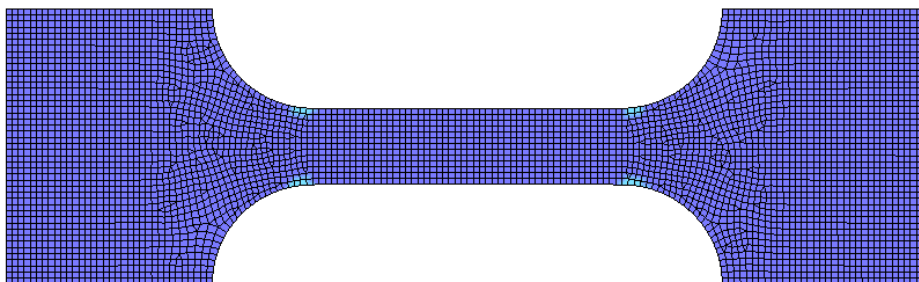


Figure 41: Tensile test simulation at 0 sec

### LS-DYNA KEYWORD DECK BY LS-PREPOST

Time = 0.04  
Contours of Effective Plastic Strain  
max ipt. value  
min=0, at elem# 20077  
max=0.00278025, at elem# 20361



Fringe Levels

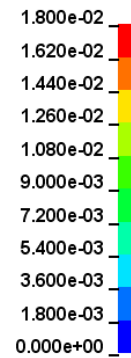
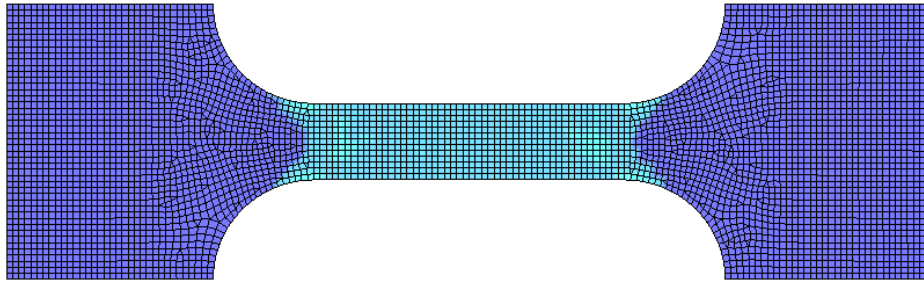


Figure 42: Tensile test simulation at 0.04 sec

**LS-DYNA KEYWORD DECK BY LS-PREPOST**

Time = 0.05  
Contours of Effective Plastic Strain  
max ipt. value  
min=0, at elem# 20077  
max=0.00519974, at elem# 20080



Fringe Levels

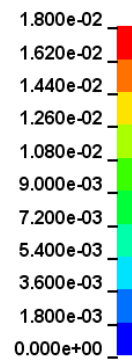
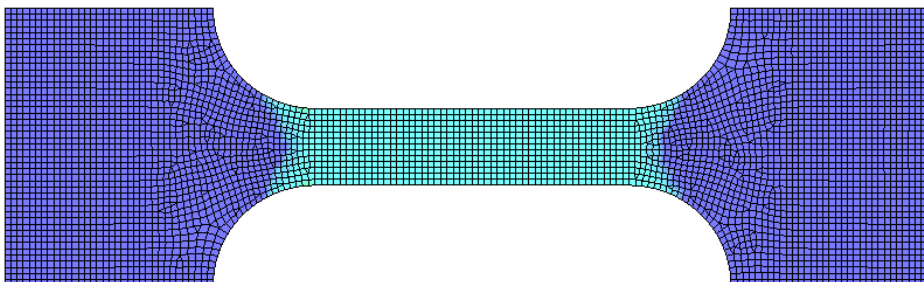


*Figure 43: Tensile test simulation at 0.05 sec*

**LS-DYNA KEYWORD DECK BY LS-PREPOST**

Time = 0.06  
Contours of Effective Plastic Strain  
max ipt. value  
min=0, at elem# 20077  
max=0.00853415, at elem# 23797



Fringe Levels



*Figure 44: Tensile test simulation at 0.06 sec*

**LS-DYNA KEYWORD DECK BY LS-PREPOST**

Time = 0.07  
Contours of Effective Plastic Strain  
max ipt. value  
min=0, at elem# 20077  
max=0.0118017, at elem# 20328

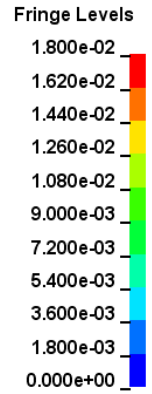
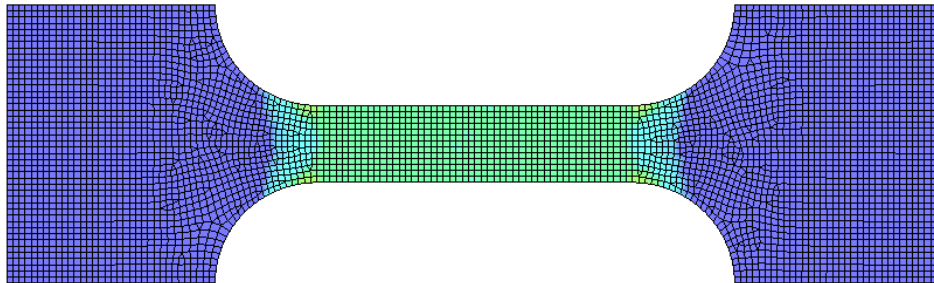


Figure 45: Tensile test simulation at 0.07 sec

**LS-DYNA KEYWORD DECK BY LS-PREPOST**

Time = 0.08  
Contours of Effective Plastic Strain  
max ipt. value  
min=0, at elem# 20077  
max=0.014912, at elem# 20328

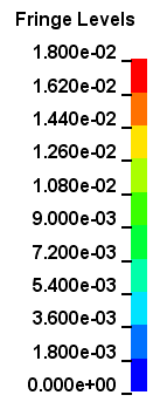
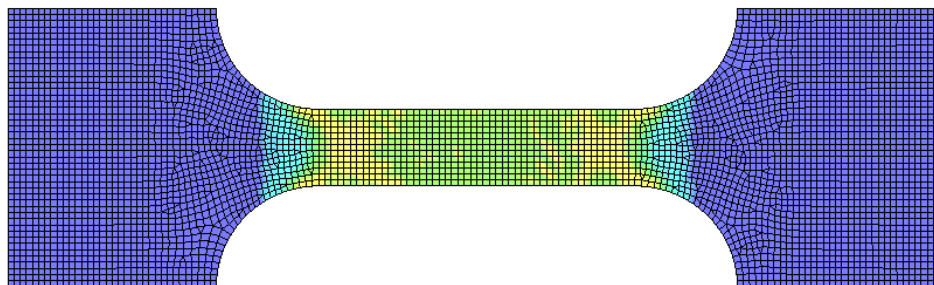


Figure 46: Tensile test simulation at 0.08 sec

**LS-DYNA KEYWORD DECK BY LS-PREPOST**

Time = 0.09  
Contours of Effective Plastic Strain  
max ipt. value  
min=0, at elem# 20077  
max=0.0176834, at elem# 20083

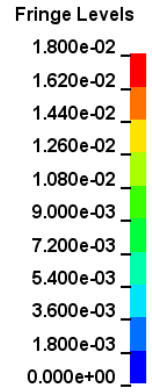
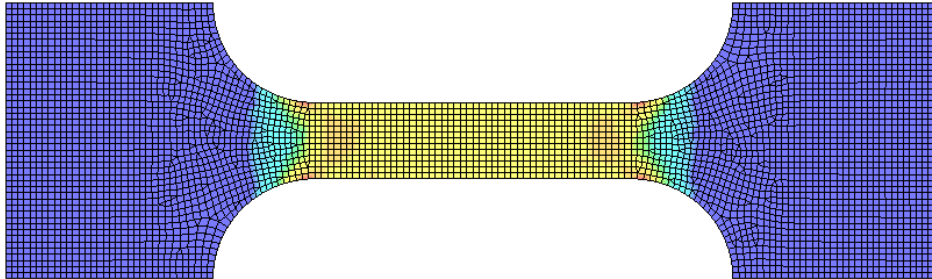


Figure 47: Tensile test simulation at 0.09 sec

**LS-DYNA KEYWORD DECK BY LS-PREPOST**

Time = 0.1  
Contours of Effective Plastic Strain  
max ipt. value  
min=0, at elem# 20077  
max=0.0179827, at elem# 20087

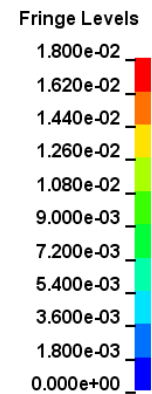
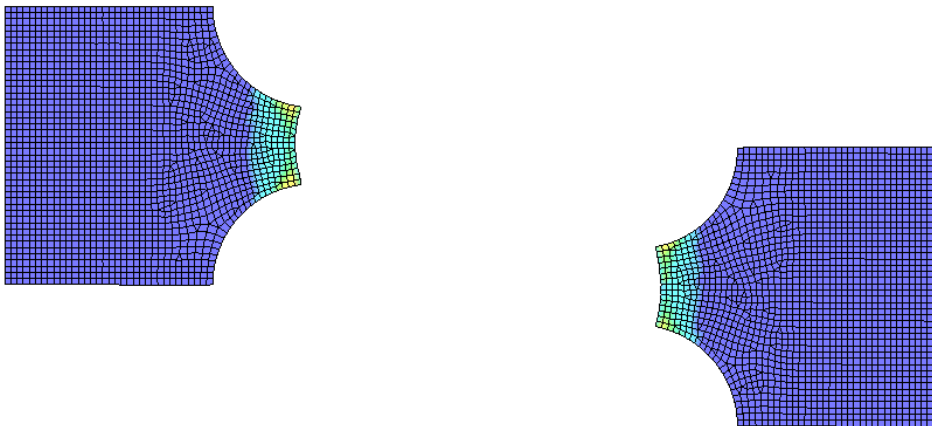


Figure 48: Tensile test simulation at 0.1 sec

### 8.3 THUMS model

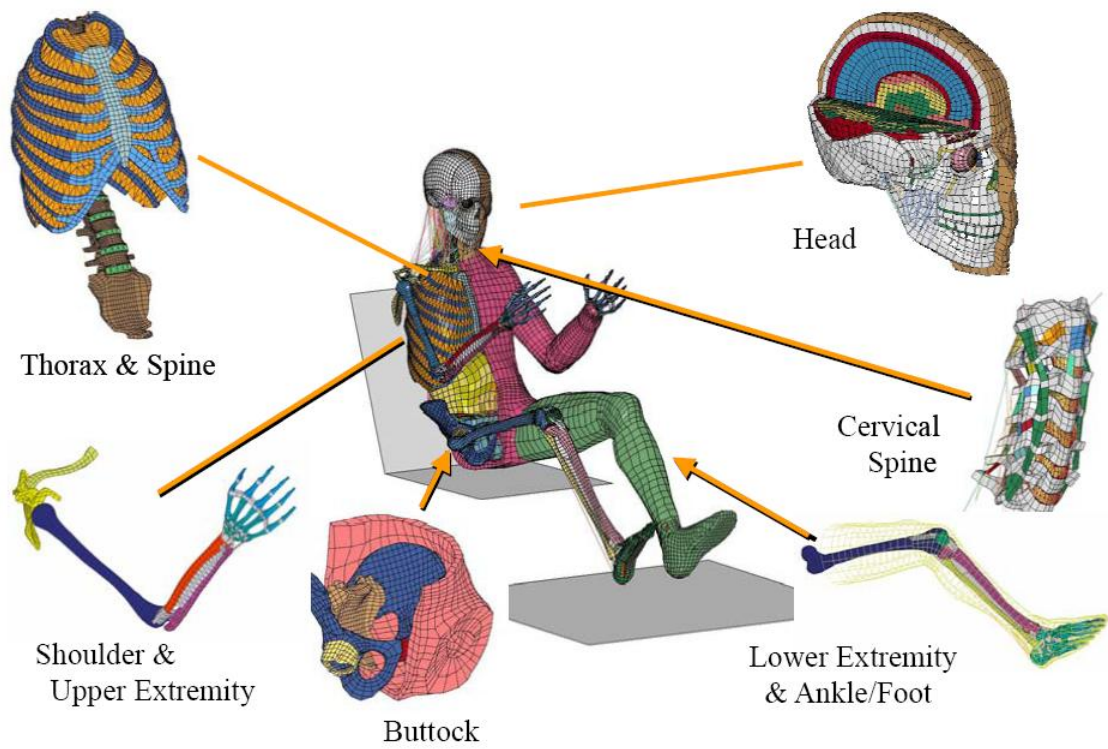


Figure 49: Composition of whole body THUMS

